Article

Cell Reports

Reciprocal Effects of Fibroblast Growth Factor Receptor Signaling on Dengue Virus Replication and Virion Production

Graphical Abstract

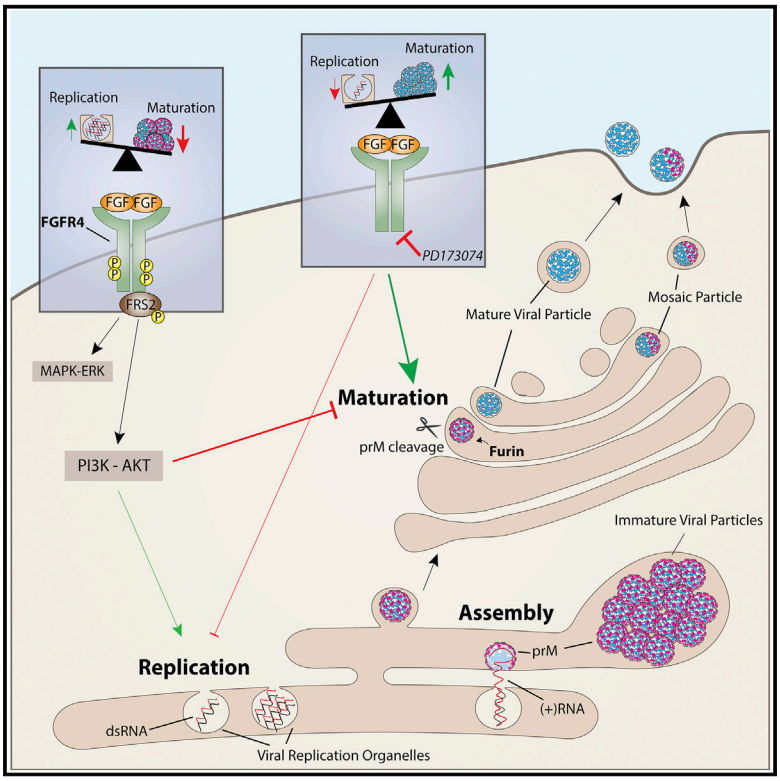

Highlights

- DENV host dependency and restriction kinases are identified through a kinome screen
- FGFR4 reciprocally affects viral replication and infectivity
- Inhibition of FGFR4 decreases replication and increases specific infectivity of virions
- Increase in specific infectivity is linked to enhanced proteolytic cleavage of prM

Authors

Mirko Cortese, Anil Kumar, Petr Matula, ..., Laurent Chatel-Chaix, Karl Rohr, Ralf Bartenschlager

Correspondence

ralf.bartenschlager@med.uni-heidelberg.de

In Brief

Cortese et al. conduct a human kinome RNAi-based screen and identify fibroblast growth factor receptor 4 (FGFR4) as a kinase that has a reciprocal effect on the DENV life cycle. Inhibition of the FGFR pathway reduces RNA replication while increasing production of infectious virus particles through enhanced proteolytic cleavage of prM.

Cortese et al., 2019, Cell Reports *27*, 2579–2592
May 28, 2019 © 2019 The Author(s).
https://doi.org/10.1016/j.celrep.2019.04.105

CellPress

Cell Reports
Article

OPEN ACCESS
CellPress

Reciprocal Effects of Fibroblast Growth Factor Receptor Signaling on Dengue Virus Replication and Virion Production

Mirko Cortese,[1,11] Anil Kumar,[1,10,11] Petr Matula,[2,7] Lars Kaderali,[3,8] Pietro Scaturro,[1,9] Holger Erfle,[4] Eliana Gisela Acosta,[1] Sandra Buehler,[1] Alessia Ruggieri,[1] Laurent Chatel-Chaix,[1,6] Karl Rohr,[2] and Ralf Bartenschlager[1,5,12,*]

[1]Department of Infectious Diseases, Molecular Virology, Heidelberg University, Im Neuenheimer Feld 344, Heidelberg 69120, Germany
[2]Biomedical Computer Vision Group, Heidelberg University, BioQuant, IPMB, and German Cancer Research Center, Im Neuenheimer Feld 267, Heidelberg 69120, Germany
[3]ViroQuant Research Group Modeling, BioQuant, Heidelberg University, Heidelberg, Germany
[4]Advanced Biological Screening Facility, BioQuant, Heidelberg University, Heidelberg 69120, Germany
[5]German Center for Infection Research, Heidelberg Partner Site, Im Neuenheimer Feld 344, Heidelberg 69120, Germany
[6]Institut National de la Recherche Scientifique, Institut Armand-Frappier, 531, Boulevard des Prairies Laval, Québec, QC H7V 1B7, Canada
[7]Present address: Faculty of Informatics, Masaryk University, Botanicka 68a, 602 00 Brno, Czech Republic
[8]Present address: University Medicine Greifswald, Institute of Bioinformatics, Walther-Rathenau-Str. 48, Greifswald 17475, Germany
[9]Present address: Technical University of Munich, School of Medicine, Institute of Virology, Schneckenburgerstr. 8, Munich 81675, Germany
[10]Present address: Department of Cell Biology, University of Alberta, Edmonton, AB, Canada
[11]These authors contributed equally
[12]Lead Contact
*Correspondence: ralf.bartenschlager@med.uni-heidelberg.de
https://doi.org/10.1016/j.celrep.2019.04.105

SUMMARY

Dengue virus (DENV) is a human arboviral pathogen accounting for 390 million infections every year. The available vaccine has limited efficacy, and DENV-specific drugs have not been generated. To better understand DENV-host cell interaction, we employed RNA interference-based screening of the human kinome and identified fibroblast growth factor receptor 4 (FGFR4) to control the DENV replication cycle. Pharmacological inhibition of FGFR exerts a reciprocal effect by reducing DENV RNA replication and promoting the production of infectious virus particles. Addressing the latter effect, we found that the FGFR signaling pathway modulates intracellular distribution of DENV particles in a PI3K-dependent manner. Upon FGFR inhibition, virions accumulate in the *trans*-Golgi network compartment, where they undergo enhanced maturation cleavage of the envelope protein precursor membrane (prM), rendering virus particles more infectious. This study reveals an unexpected reciprocal role of a cellular receptor tyrosine kinase regulating DENV RNA replication and the production of infectious virions.

INTRODUCTION

Dengue fever, hemorrhagic fever, and shock syndrome caused by infection with the dengue virus (DENV) are among the most prevalent arbovirus-associated diseases globally. According to the World Health Organization (WHO), around 40% of the world's population lives in areas endemic to this disease, with DENV causing around 100 million symptomatic infections and more than 20,000 deaths annually (Bhatt et al., 2013). In the absence of clinically approved drugs, treatment of DENV infections is only symptomatic. The existence of four antigenically distinct serotypes (DENV1–DENV4) and antibody-dependent enhancement (ADE) exacerbating secondary infection with a heterologous serotype have hindered the development of an effective prophylactic vaccine (Acosta and Bartenschlager, 2016).

The genome of DENV is a single-strand RNA of positive polarity. The genome encodes for a polyprotein that is co- and post-translationally cleaved into three structural and seven nonstructural proteins. The latter contribute to the establishment of endoplasmic reticulum (ER)-associated viral replication organelles, where the DENV genome is amplified. The structural proteins capsid (C), precursor membrane (prM), and envelope (E), together with one copy of the progeny RNA genome, form the nucleocapsid that acquires its lipid E by budding into the ER lumen. Assembled particles can often be observed as an ordered array in the ER before transport to the Golgi apparatus and subsequent secretion via the conventional secretory pathway. During this transport, maturation of DENV virions occurs via cleavage of prM within the *trans*-Golgi network (TGN) by the TGN-resident protease furin (for a detailed description of the viral replication cycle, see Neufeldt et al., 2018). This cleavage is essential to render DENV particles infectious.

Signaling cascades induced by both endogenous and exogenous stimuli influence the secretory pathway and modulate its function and organization (reviewed in Farhan and Rabouille, 2011). Key players of intracellular signaling are kinases and phosphatases. It has been suggested that more than 100 cellular

This is an open access article under the CC BY license (http://creativecommons.org/licenses/by/4.0/).

kinases and phosphatases are involved in the regulation and organization of the secretory pathway (Farhan et al., 2010).

The fibroblast growth factor receptor (FGFR) family of receptor tyrosine kinases comprises 4 highly conserved members whose signaling cascade influences several aspects of cellular homeostasis, including cell growth, proliferation, differentiation, and survival (Ornitz and Itoh, 2015). Binding of the ligand, fibroblast growth factor (FGF), induces receptor activation through dimerization and subsequent auto-phosphorylation. The main substrates of FGFR phosphorylation are phosphoinositide phospholipase Cγ (PLC-γ) and FGF receptor substrate 2α (FRS2α). FRS2α phosphorylation is required for downstream signaling through the phosphatidylinositol 3-kinase (PI3K)-AKT and the RAS-mitogen-activated protein kinase (MAPK)/extracellular signal-regulated kinase (ERK) pathways.

Like all other viruses, DENV extensively exploits host cell pathways at all steps of its replication cycle. The recently reported high-throughput RNA interference and CRISPR-Cas9-based screens, together with proteomic studies, revealed numerous host cell pathways and proteins essential for the viral replication cycle and pathogenesis of flaviviruses (Scaturro et al., 2018; Marceau et al., 2016; Zhang et al., 2016; Savidis et al., 2016; Hafirassou et al., 2017; Chatel-Chaix et al., 2016). These include essential housekeeping genes associated with viral RNA translation; polyprotein processing, e.g., by the signal peptidase (Zhang et al., 2016); and viral protein modification, e.g., by the oligosaccharyltransferase complex (Marceau et al., 2016). Additional host cell factors affecting the flaviviral replication cycle by unknown mechanisms have been reported, such as the cytosolic chaperonin-containing T complex (Hafirassou et al., 2017) and several mitochondrial proteins (Chatel-Chaix et al., 2016).

In the present study, we screened the human kinome using an RNAi-based approach to identify host cell kinases that are required for enhancing or suppressing DENV replication. Among these proteins, we identified FGFR4 as a kinase playing a reciprocal role in the DENV life cycle by promoting RNA replication but suppressing the production of infectious virus particles. The latter effect was mapped to a PI3K-dependent signaling pathway increasing the specific infectivity by enhanced maturation cleavage of prM, most likely as a result of altered intracellular trafficking of DENV particles.

RESULTS

Identification of Cellular Kinases Involved in DENV Replication via an RNAi-Based Screen

To identify kinases involved in DENV replication, high-throughput small interfering RNA (siRNA)-based screening of the human kinome was performed. The primary screening consisted of an automated, image-based, high-content assay using a library containing siRNAs targeting 719 cellular kinases. Each kinase was targeted with three independent siRNAs, alongside positive control siRNAs directed against DENV NS1 or NS3 regions of the genome and nontargeting negative controls (Figure 1A). Huh7 cells were reverse transfected on cell arrays with siRNAs for 48 h, infected with DENV2 New Guinea C (NGC) strain for 24 h, fixed, and processed for immunofluorescence analysis using an E-specific antibody (Figure 1A). Nuclear DNA was stained with DAPI and used to calculate the total number of cells in a given spot area (Figure 1B). Host dependency factors (HDFs), i.e., factors that facilitate viral replication, were considered relevant when a Z score cutoff of ≤ -1 and a p value of <0.05 were obtained; host restriction factors (HRFs), i.e., factors that impair viral replication, were pursued when a Z score cutoff of $\geq +1$ and a p value of <0.05 were reached, each with at least one siRNA. Using these criteria, 60 potential HDFs and 50 potential HRFs were selected for the validation screen (Figure 1C; Table S1). For this, three independent siRNAs from a different supplier were used to minimize off-target effects, and a Renilla-luciferase reporter virus (DV-R2A) (Fischl and Bartenschlager, 2013) derived from the DENV2 (16681 strain) was used to identify hits common between various DENV strains (Figure 1D). The analysis of the validation screen data indicated a robust performance of control siRNAs and a high correlation (Pearson correlation coefficient $\geq$ 0.8) between the replicates. Using a Z score cutoff of ≤ -2 for HDFs and $\geq +2$ for HRFs and p $\leq$ 0.05, we defined 19 HDFs and 15 HRFs (Figure 1E; Table S2).

DENV Infection Modulates the FGFR Signaling Pathway

Among the HDFs identified in this kinome screen, knockdown of FGFR4 showed a robust reduction of viral replication. For this reason, and because of the availability of inhibitors and genetic tools to study the FGFR signaling pathway, we selected this hit for further characterization. First, we assessed whether DENV infection modulates the FGFR signaling pathway (Figure 2A) by analyzing the relative abundance of basal and phosphorylated FGFR4, as well as downstream signaling molecules, using western blotting (Figure 2B). While phosphorylation levels of FGFRs were not significantly altered during the course of infection (Figure 2C, upper left panel), a strong reduction in the amounts of FGFR4 was observed at the late stage of infection (Figure 2C, top right panels). In contrast, the amount of ERK1/2 protein and its phosphorylation status did not change during this time span, arguing against general DENV-induced degradation of cellular kinases. The decrease in total FGFR4 levels was accompanied by a reduction of pFRS2α, suggesting inhibition of the downstream signaling cascade (Figure 2C, middle left panel). Although the decrease of FGFR4 abundance during the course of the infection is an unexpected feature for a HDF, our results indicate that DENV modulates the FGFR signaling pathway.

Pharmacological Inhibition of the FGFR Pathway Suppresses DENV RNA Replication and Enhances Infectious Virus Production in a PI3K-Dependent Manner

To gain insights into the role of FGFR in the DENV life cycle, we measured viral replication upon pharmacological inhibition of different steps of the FGFR signaling pathway (Figure 3A). For this purpose, we used the FGFR inhibitor PD173074. Treatment of Huh7 cells with noncytotoxic concentrations of the compound robustly downregulated the FGFR signaling pathway, as revealed by the reduction in the phosphorylation levels of the downstream kinases FRS2α and ERK1/2 (Figures S1A and S1B). To determine whether the FGFR pathway plays a role in DENV entry or RNA replication, which could not be discriminated in our RNAi-based screening assay, we used a subgenomic

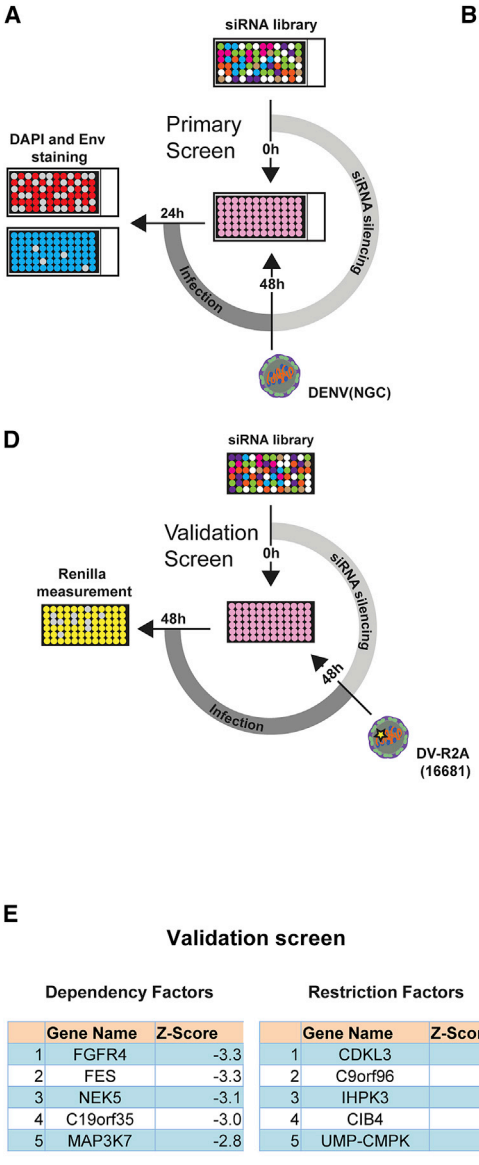

	Gene Name	Z-Score
1	FGFR4	-3.3
2	FES	-3.3
3	NEK5	-3.1
4	C19orf35	-3.0
5	MAP3K7	-2.8

	Gene Name	Z-Score
1	CDKL3	4.9
2	C9orf96	4.6
3	IHPK3	4.2
4	CIB4	4.1
5	UMP-CMPK	3.9

Figure 1. RNAi-Based Screening for Human Kinases Involved in the DENV Life Cycle

(A) Schematic representation of the primary kinome screen. Huh7 cells were reverse transfected on cell arrays with three independent siRNAs per gene, targeting in total ~700 cellular kinases. After 48 h, cells were infected with the DENV2 NGC strain (MOI = 5), harvested 24 h post-infection, and processed for immunofluorescence assay. DENV replication was measured by immunostaining against E protein.

(B) Representative images of immunostaining of positive and negative controls (a siRNA targeting NS1 and a scrambled siRNA, respectively). The envelope signal is depicted in red; nuclei is depicted in blue. The yellow circle indicates the area where the transfection mixture had been spotted.

(C) Results of the primary siRNA screen. The mean *Z* score of each siRNA is displayed in gray. Mean *Z* scores of negative and positive controls (scrambled siRNA and siRNA directed against Envelope and NS3, respectively) are shown in blue and red, respectively. The hit selection criteria ($-1 > z > 1$; $p < 0.05$) are indicated by the blue and red lines, respectively. Potential host dependency factors (HDFs) and host restriction factors (HRFs) are highlighted in light green and light blue, respectively.

(D) Setup of the validation screen. Huh7 cells were reverse transfected using three siRNAs per gene. A total of 110 primary hits were included. Forty-eight hours after transfection, cells were infected with the DV-R2A Renilla luciferase reporter virus. Viral replication was measured 48 h later by luciferase assay.

(E) List of the top five potential HDFs and HRFs from the validation screen.

See also Tables S1 and S2.

reporter replicon that was electroporated into Huh7 cells, thus bypassing the entry step. Different concentrations of the FGFR inhibitor were added immediately after electroporation, and viral replication was measured after 48 h (Figure S1C). A consistent reduction of viral RNA replication was observed. Although the magnitude of inhibition was rather low, a stronger reduction of DENV replication was found when we used infection of Huh7 cells, allowing pretreatment of the cells with the compound, which was not possible in the electroporation setting (Figure 3B). Time of addition experiments using *trans*-complemented particles, which allow only single-round infection (Scaturro et al., 2014), showed that the inhibitory effect was stronger when the compound was added before or right after infection. The inhibitory effect was gradually lost when the compound was added later during infection (Figure S1D). This kinetic argues for a role of FGFR signaling in an early step during the DENV infection cycle, such as viral RNA translation or the establishment of the membranous replication organelle.

Although replication was suppressed, the amount of infectious virus particles released from infected cells treated with the FGFR inhibitor increased up to 12-fold, indicating a reciprocal effect of FGFR signaling inhibition on DENV RNA replication and virus production (Figure 3C). In agreement with these results, activation of the FGFR signaling pathway by overexpression of the cognate FGFR ligand FGF19 increased viral replication but significantly reduced the production of infectious virus particles (Figures 3D and 3E, respectively). Cotreatment of FGF19-overexpressing cells with the FGFR inhibitor PD173074 blunted these effects, confirming the specificity of the compound (Figures 3D and 3E).

Observed phenotypes were not limited to DENV2 isolates, because FGFR inhibition increased extracellular infectivity of all DENV serotypes, as well as two strains of the Zika virus (ZIKV; MR766 and H/PF/2013) (Figures 3F and 3G). Conversely, no significant effects were observed with the related West Nile virus and Rift Valley Fever Virus (RVFV), a negative-strand RNA virus belonging to the *Phenuiviridae* family (Figure 3G and S1E,

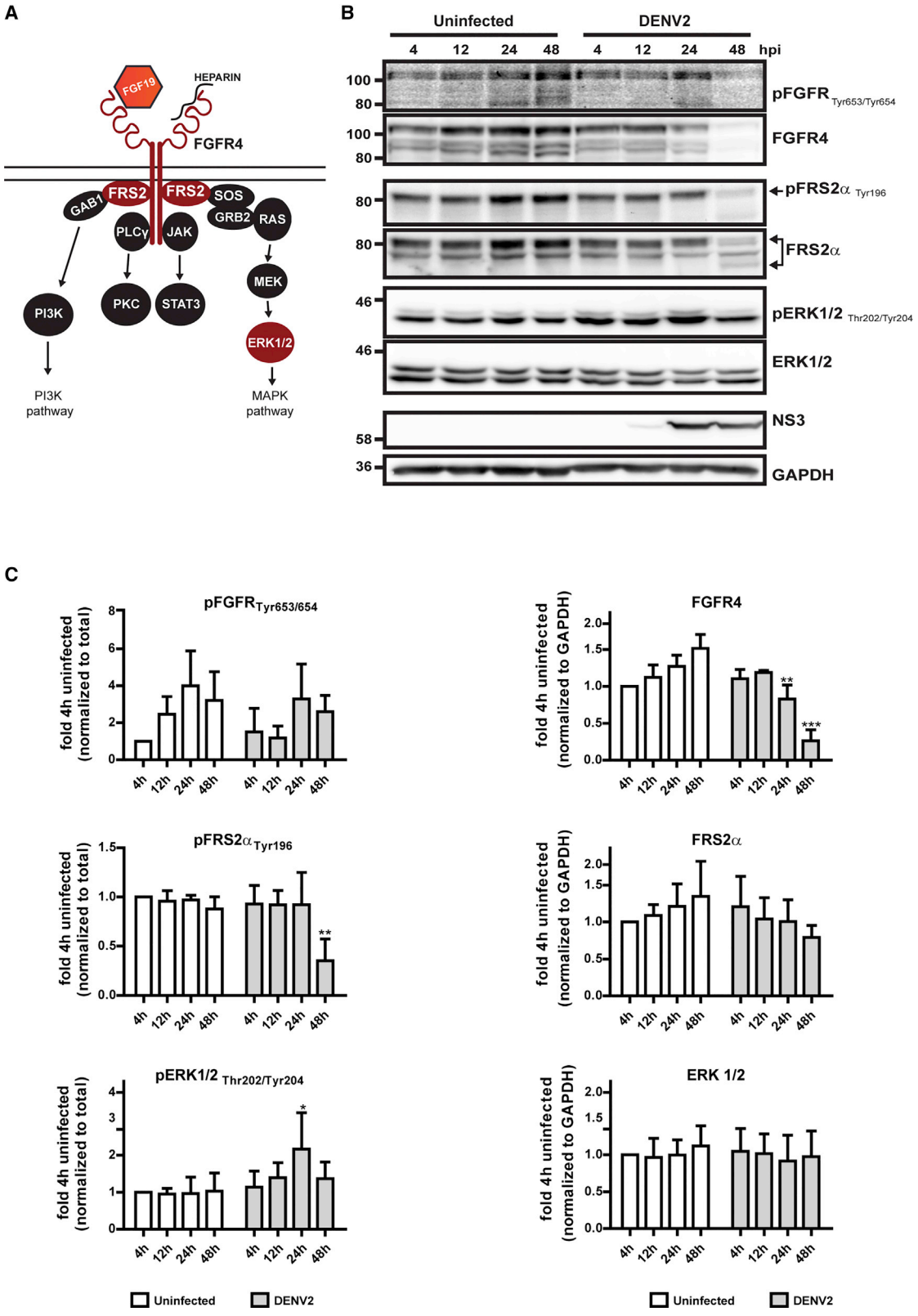

(legend on next page)

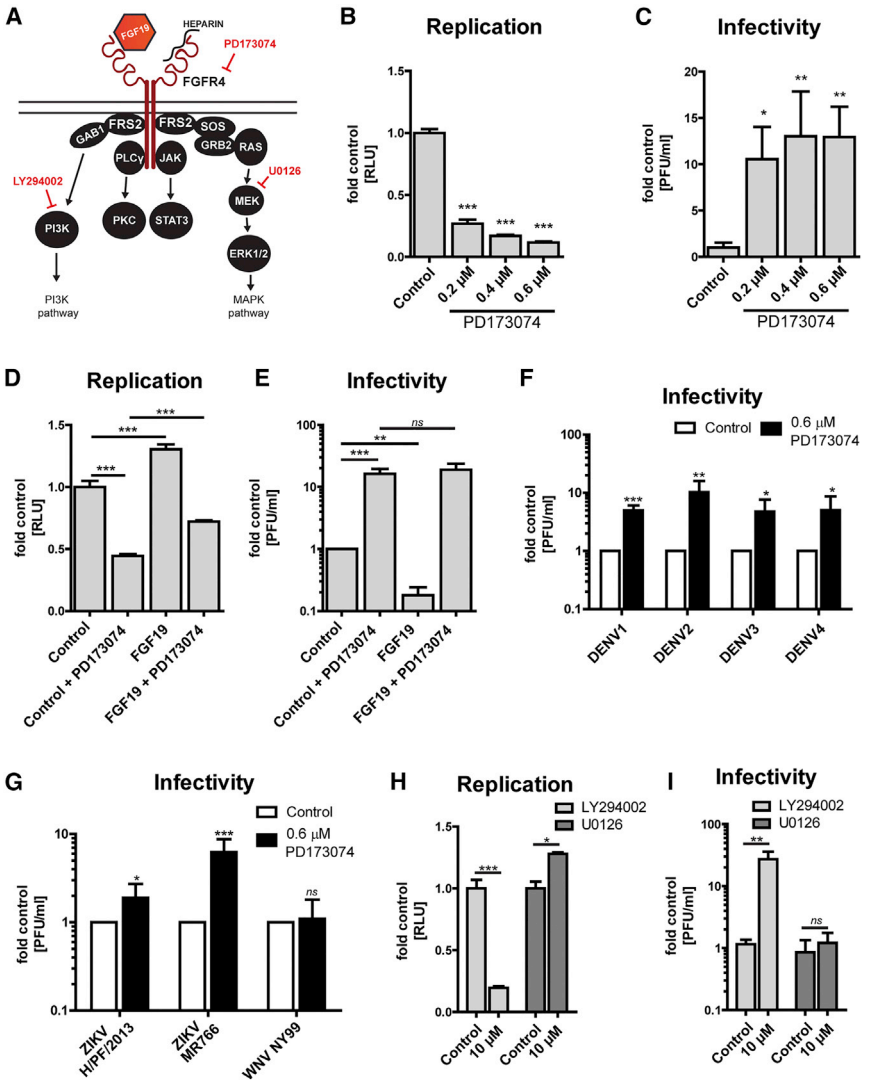

Figure 3. Pharmacological Inhibition of FGFR Reduces DENV Replication and Increases Virus Production

(A) Schematic illustration of the FGFR4 pathway. Targets of used inhibitors and agonists are indicated.

(B and C) Huh7 cells were treated for 16 h with PD173074 before infection with DV-R2A. After 48 h, replication was quantified by luciferase assay (B), and amounts of infectious virus were determined by plaque assay (C). The inhibitor was present throughout the experiment.

(D) Agonization of FGFR4 by FGF19 enhances DENV replication. Huh7 cells were transfected with a construct encoding FGF19, treated 16 h later with either DMSO or PD173074 (0.6 μM), and infected 8 h later with the DENV reporter virus. After 72 h, replication levels were measured by luciferase assay.

(E) Agonization of FGFR4 by FGF19 reduces DENV virion production. Cells were treated as in (D), and titers of the DENV reporter virus contained in the cell culture supernatant 72 h after infection were measured by plaque assay.

(F and G) Huh7 cells were pretreated for 16 h with 0.6 μM of PD173074 before infection with the indicated viruses (MOI = 0.1). After 72 h (F) or 48 h (G), titers were quantified by plaque assay.

(H and I) DENV replication and virus production in Huh7 cells pretreated with the PI3K inhibitor LY294002 or the MEK1/2 inhibitor U0126. Huh7 cells were treated overnight with indicated concentrations of the drugs, infected with DV-R2A (MOI = 1), and harvested 48 h later. Replication was measured by luciferase assay (H), whereas virus titers were quantified by plaque assay (I).

Mean and SD of two (H and I) or three (B–G) independent experiments are shown. Student's t test was used to analyze the data, except for (B) and (C), where data were analyzed with one-way ANOVA and Dunnett's post hoc test. *$p < 0.05$; **$p < 0.01$; ***$p < 0.001$. See also Figure S1.

respectively). These results suggest that FGFR signaling plays a critical role in the life cycle of all DENV serotypes, as well as some closely related flaviviruses such as ZIKV.

The FGFR signaling cascade branches through two main pathways: the MAPK pathway and the PI3K pathway (Figure 3A). To determine the effect of each pathway on DENV infectivity, we used LY294002 and U0126, two inhibitors targeting PI3K or MEK1/2, which is directly upstream of ERK, respectively (Figure 3A). Inhibition of the PI3K pathway with LY294002 mirrored the effects of FGFR inhibition, because it significantly reduced viral replication and increased the amount of released infectious virus (25-fold; $p < 0.05$) (Figures 3H and 3I, respectively). Conversely, inhibition of MEK1/2 affected viral replication only to a minor extent and had no significant effect on virus production (Figures 3H and 3I, respectively). For both compounds, no effect on cell viability was observed with used drug concentrations (Figure S1F). The effect of FGFR and PI3K pathway inhibition on DENV replication and infectivity was validated in 293T

Figure 2. DENV Infection Modulates the FGFR Signaling Pathway

(A) Schematic of the FGFR4 signaling pathway. Kinases analyzed by western blot are highlighted in brown. FRS2α, fibroblast receptor substrate 2α; GAB1, GRB2-associated-binding protein 1; PLCγ, phosphoinositide phospholipase Cγ; JAK, Janus kinase; SOS, son of sevenless; GRB2, growth factor receptor-bound protein 2; STAT3, signal transducer and activator of transcription 3; PKC, protein kinase C; PI3K, phosphatidylinositol 3-kinase.

(B) Huh7 cells were left untreated or infected with DENV2 (16681 strain; MOI = 5) and harvested at the indicated time points. Expression levels of proteins specified to the right of each panel were determined by western blot. NS3 and GAPDH were used as infection and loading controls, respectively.

(C) Levels of proteins specified at the top of each panel and detected by western blot were quantified using the ImageJ software package. All values are expressed as mean and SD from at least three independent experiments.

Data were analyzed using Student's t test. *$p < 0.05$; **$p < 0.01$; ***$p < 0.001$.

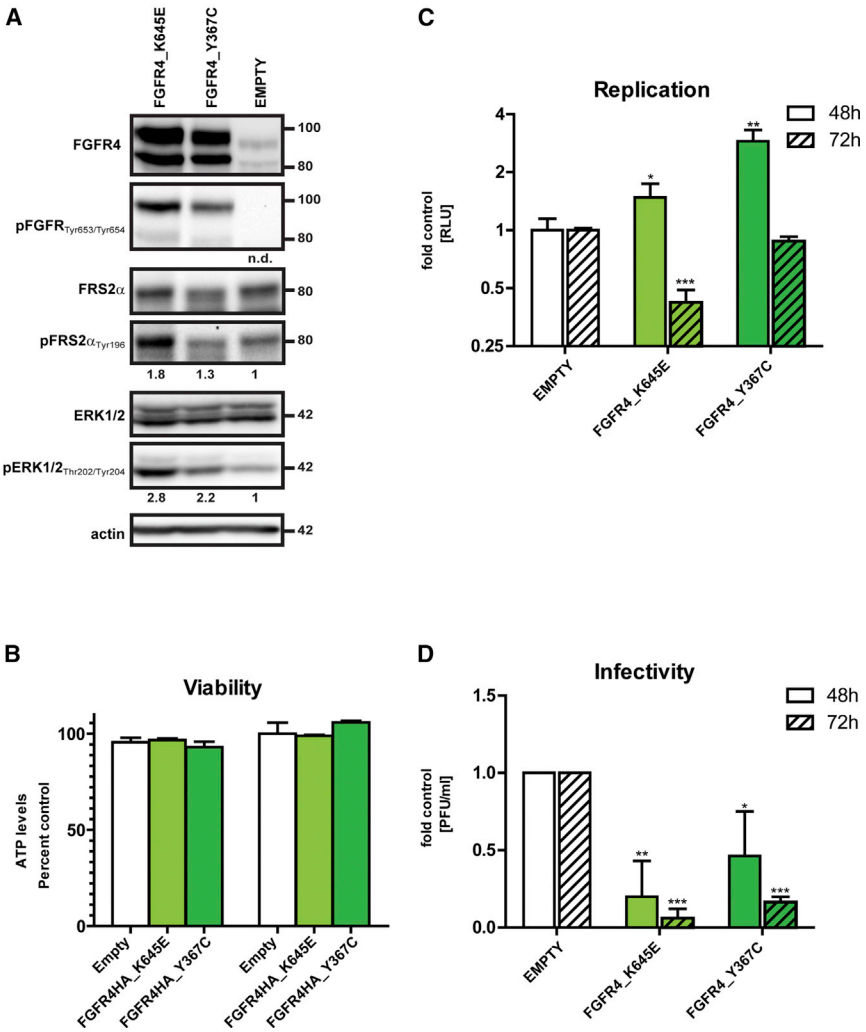

Figure 4. Enhanced FGFR4 Signaling by Overexpression of Constitutively Active Mutants Reduces the Production of Infectious DENV Particles

Huh7 cells were transduced with lentiviruses encoding indicated FGFR proteins. Three days post-transduction (dpt), cells were infected with the DV-R2A (MOI = 1).

(A) Western blots were performed 3 dpt using lysates of transduced cells. Numbers below the lanes correspond to the ratio between phospho- and total protein normalized to the empty control sample (a lentivirus encoding no heterologous protein). A representative experiment of three independent repetitions is shown.

(B) Viability of Huh7 cells as determined by measurement of ATP levels 6 days after transduction with lentiviruses encoding the indicated proteins. Means and SD from 3 technical replicates are shown.

(C) Viral replication was measured by luciferase reporter assay. Means and SD from triplicate samples are shown. Data were analyzed using Student's t test.

(D) Virus titers as determined by plaque assay. Means and SD from triplicate samples are displayed. Data were analyzed using Student's t test. *p < 0.05; **p < 0.01; ***p < 0.001.

cells and gave phenotypes similar to those observed in Huh7 cells (Figures S1G–S1I). Altogether, these results suggest that inhibition of the FGFR pathway via the PI3K branch is responsible for the reciprocal effect on DENV RNA replication and production of infectious virus particles.

Activation of FGFR4 Signaling by Constitutively Active Mutants Reduces Infectious DENV Particle Production

To corroborate our findings, we modulated FGFR signaling with a drug-independent strategy by overexpression of two constitutively active mutants of this receptor tyrosine kinase: the K645E mutant carrying an amino acid substitution in the kinase auto-inhibition loop and the FGFR4 Y367C mutant containing an additional cysteine residue in the extracellular region that induces spontaneous dimerization and receptor activation (Webster and Donoghue, 1996; Ruhe et al., 2007). Empty vector was used as control. To avoid pleiotropic effects resulting from prolonged overexpression, cells were transduced with lentiviruses, and signaling activation was assessed three days later by western blot analysis using phospho-specific antibodies. Expression of both constitutively active receptors increased the phosphorylation levels of FRS2α and ERK1/2 kinases, with no effects on cell viability (Figures 4A and 4B, respectively).

Having confirmed the activities of these FGFR mutants, cells were infected with the DENV reporter virus 3 days after lentiviral transduction, and viral replication and virus production were measured 48 and 72 h after infection using luciferase reporter and plaque assay, respectively (Figures 4C and 4D). At 48 h post-infection, stimulation of the FGFR signaling pathway via expression of both constitutively active mutants mirrored the results obtained with ligand-induced receptor activation (FGF19), with an increase in viral replication and a reduction in titers of infectious virus infectivity (Figures 4C and 4D). Extracellular infectivity decreased further 72 h post-infection and was around 17-fold lower in the case of the K645E mutant compared with empty vector-transduced cells. Consistently, at the same time point, viral replication in the culture decreased up to around 2-fold, probably due to a reduction in viral spread caused by the decreased virus titer.

These results show that activation of the FGFR pathway, through overexpression of constitutive active FGFR4, reduces the production of infectious DENV particles, consistent with data obtained by pharmacological inhibition of the FGFR4 signaling pathway.

FGFR Inhibition Enhances Specific Infectivity

The increased infectivity titers observed upon FGFR inhibition suggested increased assembly, enhanced virus release, or higher infectivity of released particles. To test for an effect on

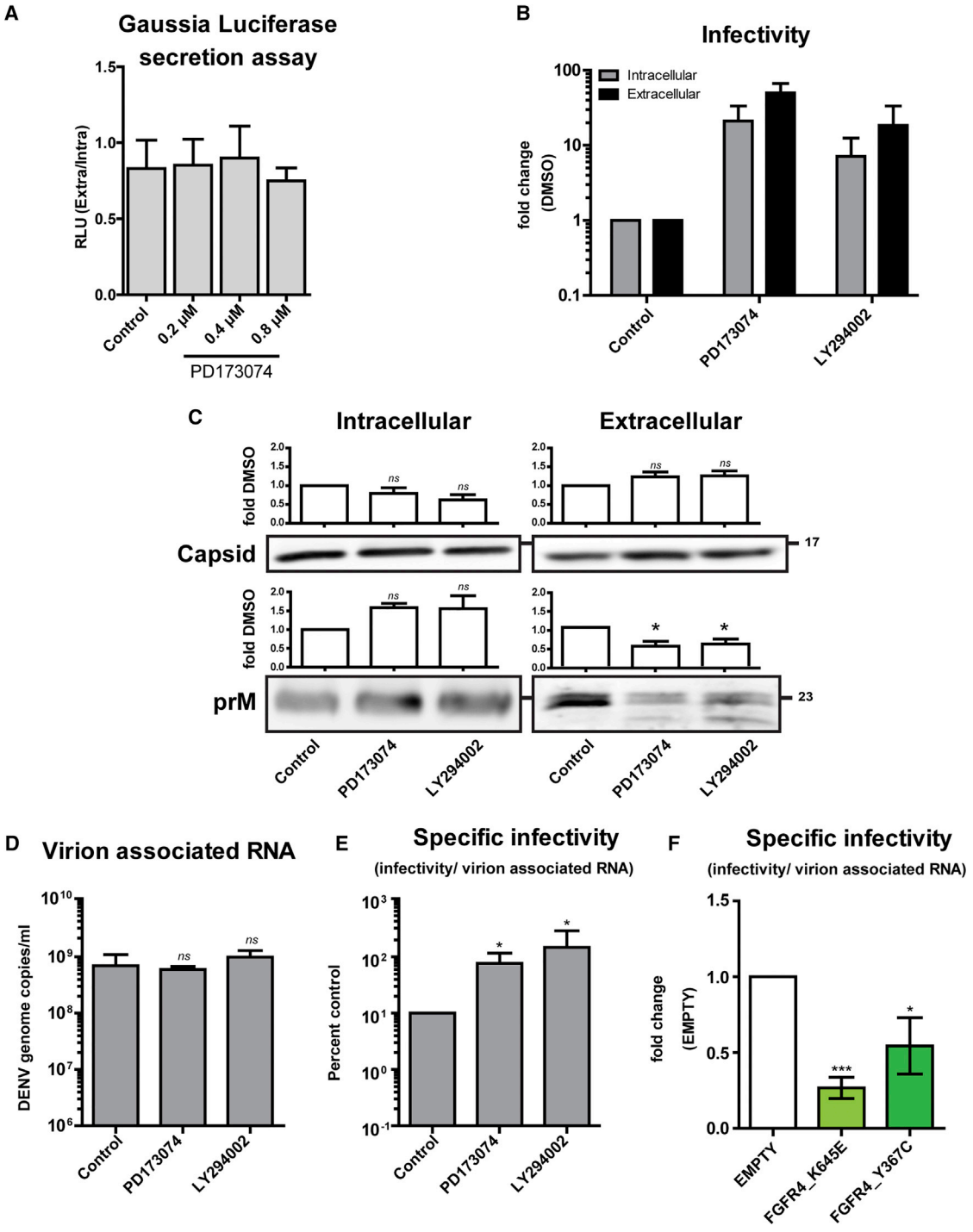

Figure 5. FGFR Inhibition Enhances the Specific Infectivity of Virus Particles

(A) Huh7 cells transfected with Gaussia luciferase reporter plasmid were treated with the indicated concentrations of PD173074 for 72 h. Gaussia luciferase activity was quantified by luciferase assay. Ratios between extra- and intracellular luciferase values are given.

(B) Huh7 cells were treated with the indicated inhibitors and infected with DENV for 72 h. Compounds were present throughout the experiment. Virus titers within cells were determined following repeated freeze-thaw cycles; extracellular virus titers were determined using culture supernatants. Values were normalized to DMSO-treated control cells.

(C) Intra- and extracellular amounts of DENV capsid and prM proteins after treatment of Huh7 cells with the indicated inhibitors for 72 h. Lower panels show representative western blots, and upper panels display the quantification of the protein signals.

(legend continued on next page)

particle release, we analyzed the impact of FGFR pathway inhibition on conventional secretion, which is the main secretory route used by DENV (Neufeldt et al., 2018). No changes of the secretion of a transiently expressed secreted version of a Gaussia luciferase were observed upon treatment with PD173074 (Figure 5A), suggesting that FGFR pathway inhibition does not affect secretion through the conventional secretory route. This finding, together with the observed increase in both intra- and extracellular infectivity upon FGFR4 inhibition (Figure 5B), rules out an effect of FGFR signaling on DENV particle release and argues for enhanced virion assembly or specific infectivity. However, treatment with the FGFR4 or PI3K inhibitor did not affect intra- and extracellular amounts of DENV C protein (Figure 5C), arguing against an increase of DENV particle assembly. Consistently, amounts of extracellular viral RNA were unaltered (Figure 5D) even though extracellular infectivity was increased (Figure 5B), indicating enhanced infectivity of DENV particles released from FGFR inhibitor-treated cells. Calculation of the ratio between extracellular virus titers and viral genomes (reflecting the number of released particles) supported this conclusion (Figure 5E). Consistently, activation of the signaling pathway by overexpression of constitutive active FGFR4 mutants decreased the specific infectivity of released particles (Figure 5F). These results provide strong evidence that FGFR plays an important role in DENV particle infectivity. In addition, the observation that the amount of extracellular prM was reduced indicated a qualitative change of the virions (Figure 5C).

FGFR Signaling Alters Intracellular Distribution of Assembled DENV Particles

Next, we sought to identify the molecular mechanism linking FGFR to the specific infectivity of DENV particles. Because FGFR signaling modulates cholesterol homeostasis and fatty acid biosynthesis (Ornitz and Itoh, 2015), modulation of this signaling pathway might alter the lipid composition of the virus particles, thus influencing their stability and infectivity. However, no changes in particle stability were observed upon either pharmacological inhibition or stimulation of the FGFR pathway, as measured by the resistance of infectious DENV particles to temperature increases or repeated freeze-thaw cycles (Figure S2).

Virus particle infectivity is tightly linked to the maturation step, which occurs in the TGN compartment and involves furin-mediated cleavage of prM to generate a mature membrane (M) protein (Neufeldt et al., 2018). Although modulation of the FGFR signaling pathway affected neither furin protein levels (Figures S3A and S3B) nor furin activity (Figures S3C and S3D), increased colocalization between prM and TGN marker TGN46 was observed, which was most evident 48 h post-infection (Figures 6A and 6B). This subcellular localization argued for altered intracellular trafficking of DENV particles, with prolonged accumulation in the TGN upon PD173074 and LY294002 treatments. Therefore, we visualized intracellular particle distribution more precisely using electron microscopy analysis of infected cells treated with FGFR or PI3K inhibitors (Figure 6C). Although we could not discriminate between mature and immature particles due to resolution limits, quantification of DENV particles residing within the rough ER, and thus by definition being immature, was possible. At 72 h post-infection, arrays of virions accumulating within virion bags, and surrounded by rough ER membrane, were readily visible in DMSO-treated samples. In agreement with our earlier findings (Welsch et al., 2009), such structures are usually close to the viral replication organelle composed of virus-induced vesicles packets (VPs) that are ER membrane invaginations into the ER lumen (Figure 6C). In drug-treated samples, the total number of virion bags within infected cells was drastically reduced, supporting the conclusion that intracellular particles are shuttled more efficiently from the ER into the secretory pathway (Figure 6D).

To corroborate this conclusion with an alternative approach, we determined the intracellular distribution of DENV within the secretory apparatus using biochemical separation of ER and Golgi membranes through a Nycodenz step gradient (Figure 7A). In drug-treated samples, higher amounts of the viral E protein cofractionated in TGN46-positive fractions compared with DMSO-treated control cells (Figure 7B). These fractions also contained the most DENV infectivity (Figure 7C), while almost no infectivity was present in Calnexin-positive ER fractions, confirming the proper separation of the intracellular membranes. Altogether, these results point toward an altered intracellular distribution of DENV particles upon FGFR signaling inhibition, resulting in an increased load of infectious DENV particles in the TGN compartment. Moreover, alteration of the intracellular distribution seems to be specific for DENV particles, because trafficking of small cargos, such as the vesicular stomatitis virus G (VSV-G) protein, was not affected by modulation of the FGFR signaling pathway (Figure S4).

FGFR Inhibition Increases Maturation of Intracellular DENV Particles

Because DENV particles undergo a maturation cleavage of prM within the TGN, we determined the amount of precursor prM and mature M proteins present on the surface of secreted virions upon FGFR or PI3K inhibitor treatment. Western blot analysis revealed a prominent band at low molecular weight consistent with mature M protein, in addition to a heavier protein reacting with the M-specific antibody and corresponding to the prM precursor (Figure 7D, left panel). Intensity of the lower band increased in drug-treated samples compared with DMSO control cells, indicating enhanced prM cleavage. To confirm the identity of these bands, immature DENV particles were generated by NH_4Cl treatment of infected cells without or with subsequent *in vitro* cleavage by recombinant furin. In the NH_4Cl-treated sample, low levels of extracellular infectivity and the absence of M confirmed the accumulation of predominantly

(D) Quantitation of DENV RNA associated with extracellular virions using qRT-PCR. Cells were treated with compounds or DMSO as specified at the bottom.
(E) Specific infectivity of DENV particles calculated as the ratio of infectious titers and number of virion-associated RNAs.
(F) Specific infectivity of virus particles released 72 h post-infection from cells expressing the different FGFR4 constructs.
Means and SD from three independent experiments are shown. Data were analyzed with Student's t test (C) and one-way ANOVA with Dunnett's post hoc test (F). *$p < 0.05$; **$p < 0.01$; ***$p < 0.001$.

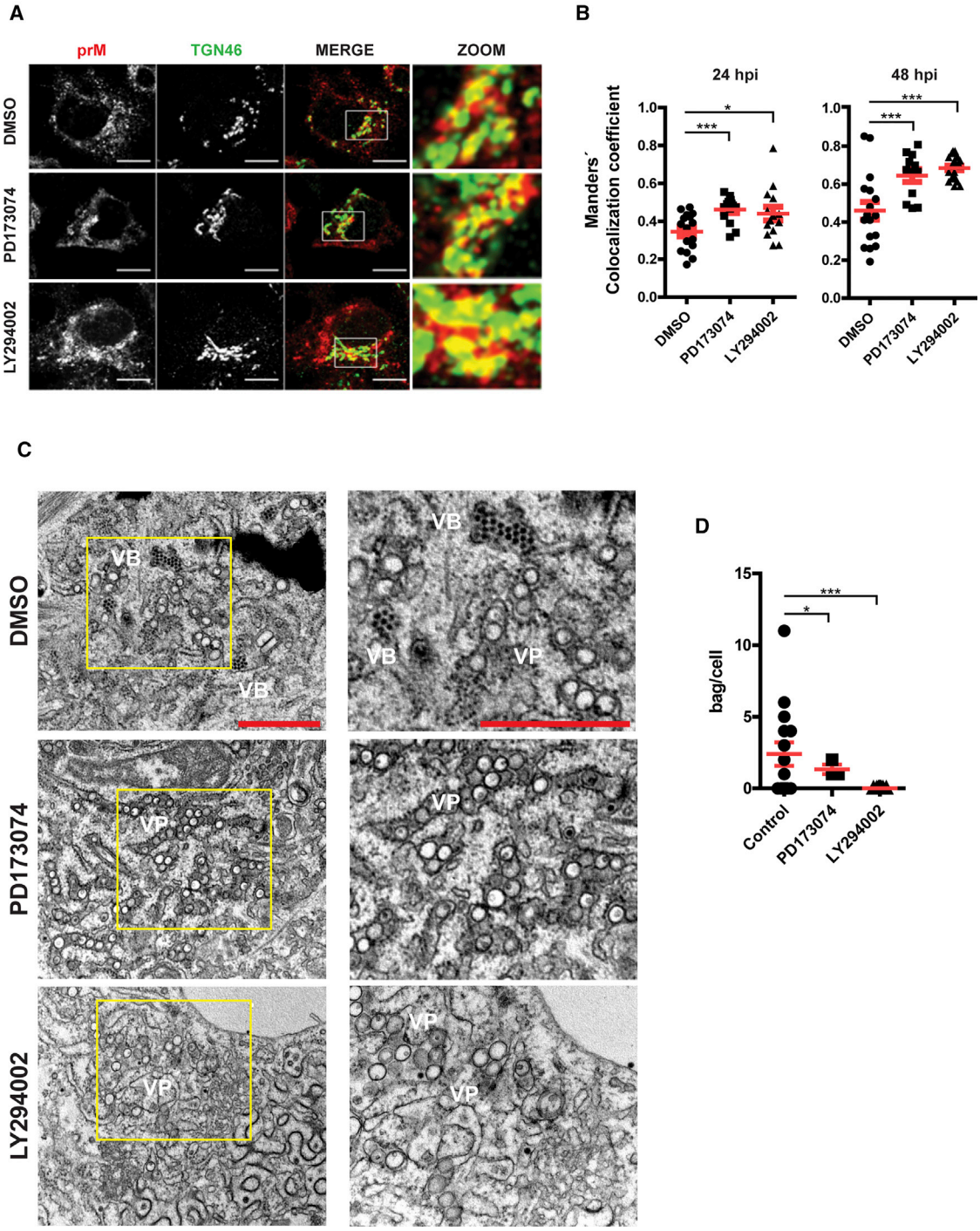

Figure 6. FGFR4 Signaling Inhibition Increases prM Accumulation in the Golgi and Reduces Accumulation of Virions in an ER-Proximal Compartment

(A) Colocalization between *trans*-Golgi network marker TGN46 and prM in Huh7 cells pretreated with DMSO or inhibitors of FGFR (PD173074) or PI3K (LY294002) and infected for 48 h with DENV. Inhibitors were kept on the cells throughout the experiment. Scale bar, 10 μm.

(B) Quantification of the colocalization using Mander's colocalization coefficients. Each dot represents one cell. Means and SD are shown. Data were analyzed using Student's t test.

(C) Cells treated with FGFR or PI3K inhibitors were infected with DENV for 72 h before processing for electron microscopy (EM) analysis. Scale bar, 1 μm. VP, vesicles packet; VB, virion bag. Yellow boxes indicate areas magnified to the right of each panel.

(D) Quantification of the number of virion bags in 15 infected cells for each condition.

Means and SD are given. See also Figures S2–S4.

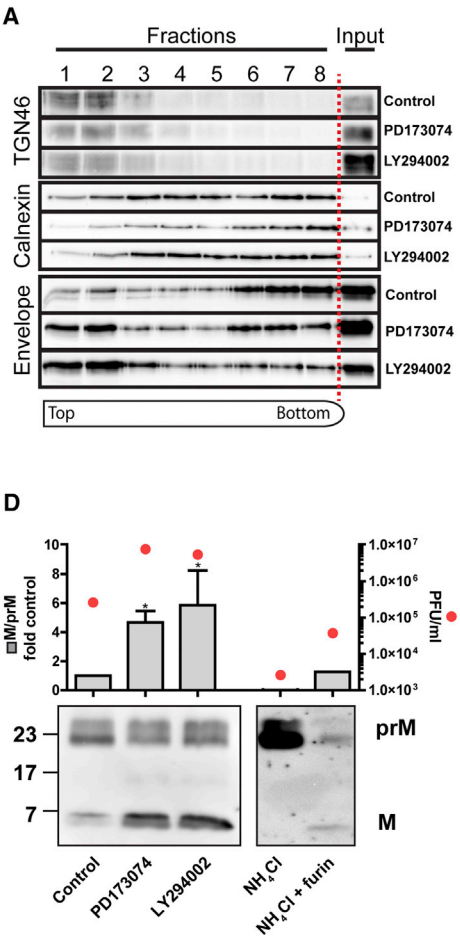

Figure 7. FGFR4 Signaling Inhibition Increases prM Maturation Cleavage

(A) Extracts of Huh7 cells treated with inhibitors of FGFR (PD173074) or PI3K (LY294002) and infected for 48 h with DENV were fractionated to separate the Golgi apparatus and ER membranes. The distribution of the indicated cellular and viral proteins was analyzed by western blotting. Inhibitors were kept on the cells throughout the experiment. The experiment was repeated twice.

(B) Quantification of the bands from (A). Shaded areas indicate TGN46 and calnexin distribution.

(C) Relative distribution of infectivity in the gradient as determined by plaque assay. For each condition, values were normalized to total infectivity.

(D) Enhanced cleavage of prM upon FGFR signaling inhibition. Cells were infected with DENV and treated with FGFR or PI3K inhibitors, treated with 20 mM NH_4Cl, or treated with NH_4Cl followed by overnight digestion with recombinant furin. Virions were purified, and prM and M were detected by western blot using a prM-specific antibody (lower panel). Quantifications of the signals are displayed in the upper panel. Values were normalized to DMSO-treated control cells (set to one). Bars represent means and SD from 3 experiments. Data were analyzed with one-way ANOVA with Dunnett's post hoc test (*$p < 0.05$). Red dots indicate virus titers as determined by plaque assay. A representative experiment from three repetitions is shown.

immature particles (Figure 7D, right panel). Upon furin treatment, a restoration of particle infectivity was observed, concomitant with the appearance of a low molecular weight protein comigrating with the one released from drug-treated cells (Figure 7D, right panel), thus confirming its identity as M.

In conclusion, these results provide compelling evidence that inhibition of the FGFR signaling pathway increases the specific infectivity of DENV particles by enhanced maturation cleavage of the prM protein in the viral E.

DISCUSSION

In this study, we screened the human kinome to identify host kinases involved in DENV replication cycle. We could identify 39 kinases promoting or restricting DENV entry or replication. The overlap between these candidates and previously reported hit lists obtained after whole-genome screenings with other flaviviruses (Savidis et al., 2016; Kwon et al., 2014) is limited. This is not unexpected, because differences in reagents and screening setups have profound effects on experimental outcomes; therefore, overlaps between hit lists from different screenings is very low in general (Savidis et al., 2016). For instance, a comparison of our screening with the siRNA-based kinome screen by Kwon and colleagues, who reported 30 kinases involved in DENV infection (Kwon et al., 2014), revealed only 2 common hits: the feline sarcoma oncogene (FES) tyrosine kinase and the casein kinase 1 delta (CSNK1D). However, while the FES kinase was identified in both screenings as a DENV restriction factor, the CSNK1D gene appears as a restriction factor in our screening but as a dependency factor in the screening by Kwon et al. (2014). Although the exact reason for this variance is not known, differences in experimental conditions most likely account for this discrepancy. In yet another screen employing small molecule inhibitors of cellular tyrosine kinases to identify pathways exploited by DENV during its life cycle, the Src family of kinases, and in particular the Fyn kinase, were found to play a role in viral replication (Chu and Yang, 2007; de Wispelaere et al., 2013).

Among the kinases identified in the present study, we focused our attention on FGFR4. Members of the FGFR family have been previously identified as host factors involved in the replication of several viruses. For instance, knockdown of FGFR4 was reported to limit influenza virus entry and replication, while knockdown of FGFR1 promoted its replication (König et al., 2010; Liu et al., 2015). Moreover, ligand-induced stimulation of the FGFR pathway inhibited replication of Coxsackievirus and vesicular stomatitis virus (van Asten et al., 2018). Here we show that several flaviviruses (all four DENV serotypes and two ZIKV lineages) are influenced by FGFR signaling. Inhibition of the FGFR4 signaling pathway had a reciprocal effect by dampening DENV replication and stimulating virus particle maturation, which is mediated, at least partly, by increasing prM cleavage. Similar

results were obtained by inhibition of PI3K, arguing that the PI3K arm of the FGFR4 pathway confers this effect. Activation of the pathway by the natural ligand FGF19 or by overexpression of constitutive active FGFR4 mutants markedly reduced virus infectivity, thus confirming the specificity of the FGFR inhibitor treatment. We observed a reduction in FGFR4 protein abundance, together with a decrease in the phosphorylation levels of the adaptor protein FRS2α, at late time points after infection, whereas the amounts of the downstream kinase ERK1/2 were not affected. Therefore, we conclude that FGFR4 signaling is impaired during DENV infection specifically at the level of the membrane receptor but does not affect all kinases of this pathway. This observation might be counterintuitive, given that FGFR4 was identified as a dependency factor promoting DENV RNA replication. However, the inhibition of RNA replication induced by the inhibition of the FGFR signaling pathway is gradually lost with extended time spans after infection. This observation supports the assumption that FGFR promotes DENV RNA replication at an early time point after infection, e.g., to establish the viral replication organelle, while later, when replication is at a steady state, the FGFR pathway is no longer required for RNA amplification but instead is a disadvantage for high-level production of infectious virus particles. Our siRNA-based screen was designed to identify host factors of relevance for viral entry and replication, because we used high MOI infection and analyzed cells 24 h post-infection, i.e., conditions under which virus spread had not occurred. Therefore, FGFR4 was identified as a dependency factor promoting DENV RNA replication.

Ligand-induced dimerization activates the FGFR signaling cascade that branches through four major signaling pathways: PLCγ-protein kinase C (PKC), signal transducer and activator of transcription (STAT), RAS-MAPK, and PI3K-AKT. The latter two rely on the docking protein FRS2α that constitutively associates with the membrane proximal region of FGFR and acts as a docking platform for downstream effector proteins (Gotoh, 2008). Because phosphorylation of FRS2α decreases at late time points after infection, one might assume that signaling inhibition through the RAS-MAPK or the PI3K-AKT pathway might influence DENV replication. Inhibition of PI3K with LY294002 recapitulated the effect observed upon FGFR blockade, i.e., a reduction of viral replication and an increase of virus production. In contrast, treatment with the ERK inhibitor U0126, previously shown to inhibit the replication of DENV2 and other members of the *Flaviviridae* family, such as yellow fever virus (YFV) and hepatitis C virus (HCV) (Albarnaz et al., 2014; Zhao et al., 2015), had no effect in our experimental setup.

Infection with DENV and Japanese encephalitis virus (JEV) or expression of the West Nile virus (WNV) C protein was shown to increase phosphorylation of the AKT kinase early during infection through a PI3K-dependent mechanism to inhibit apoptosis (Lee et al., 2005; Urbanowski and Hobman, 2013). As a result, inhibition of PI3K enhanced death of infected cells. Although there is evidence that the PI3K-AKT axis promotes survival of flavivirus-infected cells, the outcome of PI3K inhibition appears to depend on the particular virus and cell culture system used. For instance, treatment of mouse neuroblastoma cells or human lung epithelial cells with LY294002 was reported to have no effect on DENV and JEV replication or particle production (Lee et al., 2005). In the case of WNV, an increase of infectivity was observed upon PI3K inhibition with the same compound (Wang et al., 2017). Although we do not exclude a role of FGFR signaling in DENV-induced cytopathic effects, our data suggest that the inhibition of PI3K reduced DENV replication while increasing specific infectivity. This phenotype was not observed upon inhibition of the downstream effector kinase AKT (data not shown), suggesting that PI3K enhances DENV infectivity by an AKT-independent pathway. In any case, the increase in extracellular infectivity as reported here was not due to a general augmentation of the conventional secretory pathway, because release of the Gaussia luciferase reporter was not affected. Enhanced infectivity was also not due to an increase of virus particle assembly, because the levels of DENV RNA and E released from cells were unaltered by FGFR inhibitor treatment. Instead, the specific infectivity of DENV particles was profoundly increased upon FGFR pathway inhibition. In principle, two mechanisms could account for enhanced infectivity. The first one is an alteration of the lipid composition of virus particles, which has previously been shown to affect virion stability and specific infectivity (Gullberg et al., 2018). Consistently, FGFR4 activation regulates cholesterol synthesis (Tang et al., 2018), while signaling via FGFR3 was shown to increase fatty acid synthesis in cancer cells (Du et al., 2012). However, we found that stability of DENV particles collected from FGFR inhibitor-treated cells was not affected, arguing against an effect of the physical properties of the viral lipid E. Still, alterations of the lipid composition of the viral replication organelle might explain the reduction of viral RNA replication observed upon inhibition of the FGFR signaling pathway. Distinct lipids are likely required to create the energetically favorable microenvironment necessary to induce ER membrane curvature and formation of the invaginated vesicles constituting the flaviviral replication organelle (Leier et al., 2018). Lipidomic studies have highlighted an increase in ceramides and other classes of sphingolipids upon flavivirus infection (Martín-Acebes et al., 2014; Perera et al., 2012). In addition, cholesterol has been shown to be essential for flaviviral replication (Leier et al., 2018). Thus, modulation of this pathway might affect the availability of distinct lipids essential for the formation of the viral replication organelle.

A second mechanism that could explain the increased specific infectivity of DENV particles upon FGFR pathway inhibition is enhanced particle maturation. During flavivirus assembly, immature virions form by budding into the ER lumen and are secreted via transport through the Golgi apparatus (Neufeldt et al., 2018). Structural rearrangements of the viral surface glycoproteins, upon exposure to the acidic milieu of the TGN, allow for the recognition of a cleavage motif in prM by the TGN-resident protease furin (Neufeldt et al., 2018). The presence of a suboptimal furin cleavage motif in DENV prM results in the production of highly heterogeneous mosaic particles that display different grades of maturation (Junjhon et al., 2008). Thus, variations in both the prM sequence and the furin expression levels can affect particle maturation. We did not observe an increase in furin expression or enzymatic activity upon modulation of the FGFR pathway. However, we observed a higher amount of prM and E in the TGN upon FGFR inhibition using two complementary approaches, i.e.,

biochemical fractionation and light microscopy. Therefore, it is tempting to speculate that intracellular trafficking of DENV particles is altered upon FGFR signaling inhibition. Consistently, less immature virions were detected in infected and drug-treated cells, as deduced from the lower number of virion bags, corresponding to dilated ER cisternae that contain regular arrays of virus particles (Welsch et al., 2009). While the exact role of these structures is uncertain, virion bags might be an intracellular reservoir of immature assembled particles to be delivered to the TGN. This assumption supports the hypothesis that the rate-limiting step of DENV secretion is ER-to-Golgi trafficking and that this process might be affected by FGFR signaling. However, the FGFR signaling phenotype reported here is not due to increased particle secretion rate but rather is the result of enhanced prM cleavage, correlating with prolonged accumulation of virions in the TGN and thus facilitating furin-mediated cleavage. Moreover, the influence of FGFR on intracellular trafficking seems to be specific to DENV, because transport of small cargo such as the VSV-G is not affected. Alternatively, FGFR signaling has been reported to alter Golgi morphogenesis, as well as mannose 6-phosphate receptor trafficking and recycling between the TGN and the plasma membrane (Anitei et al., 2014). Therefore, FGFR inhibition might alter the trafficking of furin to increase local abundance in those cellular compartments containing immature DENV particles. However, a mechanistic link between the alteration of virion trafficking and the increase in prM maturation upon FGFR pathway inhibition needs to be established. We cannot exclude other mechanisms that might be responsible for increased particle infectivity, such as modulation of the pH in organelles and vesicles of the secretory pathway or altered particle assembly.

In conclusion, we report a novel role of FGFR signaling in reciprocally regulating DENV RNA replication and virion maturation. Given this opposing effect and the reduction of FGFR4 protein levels observed during the time course of infection, it is tantalizing to speculate that the FGFR pathway might act as a regulator, contributing to an early-late switch of the viral life cycle. Early in infection, when FGFR4 levels are high, RNA replication is favored; in contrast, at a late stage of infection, when FGFR4 levels and thus FGFR signaling are low, production of infectious virus particles is favored by enhancing the maturation cleavage of prM. The reciprocal role of FGFR4 reported here illustrates the versatile strategies developed by viruses to exploit in time and space the host machineries and signaling pathways for the benefit of efficient propagation.

STAR★METHODS

Detailed methods are provided in the online version of this paper and include the following:

- KEY RESOURCES TABLE
- CONTACT FOR REAGENT AND RESOURCE SHARING
- EXPERIMENTAL MODEL AND SUBJECT DETAILS
  - Cell lines and culture conditions
  - Viruses
- METHOD DETAILS
  - Plasmid constructions
  - Primary siRNA Screening
  - Validation siRNA screening
  - Electroporation of DENV RNA
  - Virus replication assays
  - RNA quantification by RT-qPCR
  - Indirect immunofluorescence
  - Lentivirus production and FGFR4 overexpression
  - Generation of trans-complemented DENV particles
  - Generation of furin KO cells
  - Electron microscopy
  - Cell fractionation
  - Furin cleavage assay
  - Furin enzyme activity assay
  - VSV-G trafficking assay
- QUANTIFICATION AND STATISTICAL ANALYSIS

SUPPLEMENTAL INFORMATION

Supplemental Information can be found online at https://doi.org/10.1016/j.celrep.2019.04.105.

ACKNOWLEDGMENTS

We are grateful to the Electron Microscopy Core Facility at Heidelberg University, headed by Stefan Hillmer; the Infectious Diseases Imaging Platform (IDIP) at the Center for Integrative Infectious Disease Research in Heidelberg, headed by Vibor Laketa; and Ulrike Engel and Christian Ackermann at the Nikon Imaging Center (Heidelberg University) for support and access to their equipment. We are also grateful to Ulrike Herian, Stephanie Kallis, Marie Bartenschlager, and Fredy Huschmand for technical support and Volker Lohmann and Christopher J. Neufeldt for helpful discussions. We thank the European Virus Archive goes Global (EVAg) and Xavier de Lamballerie (Emergence des Pathologies Virales, Aix-Marseille University) for providing ZIKV MR766 and H/PF/2013 original stocks. We are grateful to Andrew Davidson for providing the DV-NGC-encoding plasmid, to Didier Trono (EPFL, Lausanne, Switzerland) for providing the lentivirus packaging constructs, and to Megan Stanifer for help with the VSV-G assay. This work was supported by the Deutsche Forschungsgemeinschaft (SFB1129, TP11, and BA1505/8-1) to R.B. E.G.A. was supported by the Humboldt Foundation. P.M. is grateful to the Ministry of Education, Youth and Sports (CZ.02.1.01/0.0/0.0/16_013/0001775) for financial support. The Advanced Biological Screening Facility is supported by the CellNetworks-Cluster of Excellence (EXC81).

AUTHOR CONTRIBUTIONS

Conceptualization & Methodology, M.C., A.K., and R.B.; Formal Analysis, L.K., P.M., and K.R.; Investigation, M.C., A.K., L.C.-C., E.G.A., P.S., S.B., and A.R.; Resources, H.E.; Writing – Original Draft, M.C. and R.B.; Writing – Review & Editing, M.C., A.K., and R.B.; Funding Acquisition, R.B.

DECLARATION OF INTERESTS

The authors declare no competing interests.

Received: December 21, 2018
Revised: March 27, 2019
Accepted: April 23, 2019
Published: May 28, 2019

REFERENCES

Acosta, E.G., and Bartenschlager, R. (2016). Paradoxical role of antibodies in dengue virus infections: considerations for prophylactic vaccine development. Expert Rev. Vaccines *15*, 467–482.

Albarnaz, J.D., De Oliveira, L.C., Torres, A.A., Palhares, R.M., Casteluber, M.C., Rodrigues, C.M., Cardozo, P.L., De Souza, A.M., Pacca, C.C., Ferreira, P.C., et al. (2014). MEK/ERK activation plays a decisive role in yellow fever virus replication: implication as an antiviral therapeutic target. Antiviral Res. *111*, 82–92.

Anitei, M., Chenna, R., Czupalla, C., Esner, M., Christ, S., Lenhard, S., Korn, K., Meyenhofer, F., Bickle, M., Zerial, M., and Hoflack, B. (2014). A high-throughput siRNA screen identifies genes that regulate mannose 6-phosphate receptor trafficking. J. Cell Sci. *127*, 5079–5092.

Bär, S., Rommelaere, J., and Nüesch, J.P. (2013). Vesicular transport of progeny parvovirus particles through ER and Golgi regulates maturation and cytolysis. PLoS Pathog. *9*, e1003605.

Bhatt, S., Gething, P.W., Brady, O.J., Messina, J.P., Farlow, A.W., Moyes, C.L., Drake, J.M., Brownstein, J.S., Hoen, A.G., Sankoh, O., et al. (2013). The global distribution and burden of dengue. Nature *496*, 504–507.

Chatel-Chaix, L., Fischl, W., Scaturro, P., Cortese, M., Kallis, S., Bartenschlager, M., Fischer, B., and Bartenschlager, R. (2015). A Combined Genetic-Proteomic Approach Identifies Residues within Dengue Virus NS4B Critical for Interaction with NS3 and Viral Replication. J. Virol. *89*, 7170–7186.

Chatel-Chaix, L., Cortese, M., Romero-Brey, I., Bender, S., Neufeldt, C.J., Fischl, W., Scaturro, P., Schieber, N., Schwab, Y., Fischer, B., et al. (2016). Dengue Virus Perturbs Mitochondrial Morphodynamics to Dampen Innate Immune Responses. Cell Host Microbe *20*, 342–356.

Chu, J.J., and Yang, P.L. (2007). c-Src protein kinase inhibitors block assembly and maturation of dengue virus. Proc. Natl. Acad. Sci. USA *104*, 3520–3525.

Cortese, M., Goellner, S., Acosta, E.G., Neufeldt, C.J., Oleksiuk, O., Lampe, M., Haselmann, U., Funaya, C., Schieber, N., Ronchi, P., et al. (2017). Ultrastructural Characterization of Zika Virus Replication Factories. Cell Rep. *18*, 2113–2123.

de Wispelaere, M., LaCroix, A.J., and Yang, P.L. (2013). The small molecules AZD0530 and dasatinib inhibit dengue virus RNA replication via Fyn kinase. J. Virol. *87*, 7367–7381.

Du, X., Wang, Q.R., Chan, E., Merchant, M., Liu, J., French, D., Ashkenazi, A., and Qing, J. (2012). FGFR3 stimulates stearoyl CoA desaturase 1 activity to promote bladder tumor growth. Cancer Res. *72*, 5843–5855.

DuBridge, R.B., Tang, P., Hsia, H.C., Leong, P.M., Miller, J.H., and Calos, M.P. (1987). Analysis of mutation in human cells by using an Epstein-Barr virus shuttle system. Mol. Cell. Biol. *7*, 379–387.

Erfle, H., Neumann, B., Liebel, U., Rogers, P., Held, M., Walter, T., Ellenberg, J., and Pepperkok, R. (2007). Reverse transfection on cell arrays for high content screening microscopy. Nat. Protoc. *2*, 392–399.

Farhan, H., and Rabouille, C. (2011). Signalling to and from the secretory pathway. J. Cell Sci. *124*, 171–180.

Farhan, H., Wendeler, M.W., Mitrovic, S., Fava, E., Silberberg, Y., Sharan, R., Zerial, M., and Hauri, H.P. (2010). MAPK signaling to the early secretory pathway revealed by kinase/phosphatase functional screening. J. Cell Biol. *189*, 997–1011.

Fischl, W., and Bartenschlager, R. (2013). High-throughput screening using dengue virus reporter genomes. Methods Mol. Biol. *1030*, 205–219.

Gotoh, N. (2008). Regulation of growth factor signaling by FRS2 family docking/scaffold adaptor proteins. Cancer Sci. *99*, 1319–1325.

Gualano, R.C., Pryor, M.J., Cauchi, M.R., Wright, P.J., and Davidson, A.D. (1998). Identification of a major determinant of mouse neurovirulence of dengue virus type 2 using stably cloned genomic-length cDNA. J. Gen. Virol. *79*, 437–446.

Gullberg, R.C., Steel, J.J., Pujari, V., Rovnak, J., Crick, D.C., and Perera, R. (2018). Stearoly-CoA desaturase 1 differentiates early and advanced dengue virus infections and determines virus particle infectivity. PLoS Pathog. *14*, e1007261.

Hafirassou, M.L., Meertens, L., Umaña-Diaz, C., Labeau, A., Dejarnac, O., Bonnet-Madin, L., Kümmerer, B.M., Delaugerre, C., Roingeard, P., Vidalain, P.O., and Amara, A. (2017). A Global Interactome Map of the Dengue Virus NS1 Identifies Virus Restriction and Dependency Host Factors. Cell Rep. *21*, 3900–3913.

Junjhon, J., Lausumpao, M., Supasa, S., Noisakran, S., Songjaeng, A., Saraithong, P., Chaichoun, K., Utaipat, U., Keelapang, P., Kanjanahaluethai, A., et al. (2008). Differential modulation of prM cleavage, extracellular particle distribution, and virus infectivity by conserved residues at nonfurin consensus positions of the dengue virus pr-M junction. J. Virol. *82*, 10776–10791.

König, R., Stertz, S., Zhou, Y., Inoue, A., Hoffmann, H.H., Bhattacharyya, S., Alamares, J.G., Tscherne, D.M., Ortigoza, M.B., Liang, Y., et al. (2010). Human host factors required for influenza virus replication. Nature *463*, 813–817.

Kwon, Y.J., Heo, J., Wong, H.E., Cruz, D.J., Velumani, S., da Silva, C.T., Mosimann, A.L., Duarte Dos Santos, C.N., Freitas-Junior, L.H., and Fink, K. (2014). Kinome siRNA screen identifies novel cell-type specific dengue host target genes. Antiviral Res. *110*, 20–30.

Lee, C.J., Liao, C.L., and Lin, Y.L. (2005). Flavivirus activates phosphatidylinositol 3-kinase signaling to block caspase-dependent apoptotic cell death at the early stage of virus infection. J. Virol. *79*, 8388–8399.

Leier, H.C., Messer, W.B., and Tafesse, F.G. (2018). Lipids and pathogenic flaviviruses: An intimate union. PLoS Pathog. *14*, e1006952.

Liu, X., Lai, C., Wang, K., Xing, L., Yang, P., Duan, Q., and Wang, X. (2015). A Functional Role of Fibroblast Growth Factor Receptor 1 (FGFR1) in the Suppression of Influenza A Virus Replication. PLoS ONE *10*, e0124651.

Livak, K.J., and Schmittgen, T.D. (2001). Analysis of relative gene expression data using real-time quantitative PCR and the 2(-Delta Delta C(T)) Method. Methods *25*, 402–408.

Marceau, C.D., Puschnik, A.S., Majzoub, K., Ooi, Y.S., Brewer, S.M., Fuchs, G., Swaminathan, K., Mata, M.A., Elias, J.E., Sarnow, P., and Carette, J.E. (2016). Genetic dissection of Flaviviridae host factors through genome-scale CRISPR screens. Nature *535*, 159–163.

Martín-Acebes, M.A., Merino-Ramos, T., Blázquez, A.B., Casas, J., Escribano-Romero, E., Sobrino, F., and Saiz, J.C. (2014). The composition of West Nile virus lipid envelope unveils a role of sphingolipid metabolism in flavivirus biogenesis. J. Virol. *88*, 12041–12054.

Matula, P., Kumar, A., Wörz, I., Erfle, H., Bartenschlager, R., Eils, R., and Rohr, K. (2009). Single-cell-based image analysis of high-throughput cell array screens for quantification of viral infection. Cytometry A *75*, 309–318.

Miller, S., Sparacio, S., and Bartenschlager, R. (2006). Subcellular localization and membrane topology of the Dengue virus type 2 Non-structural protein 4B. J. Biol. Chem. *281*, 8854–8863.

Nakabayashi, H., Taketa, K., Miyano, K., Yamane, T., and Sato, J. (1982). Growth of human hepatoma cells lines with differentiated functions in chemically defined medium. Cancer Res. *42*, 3858–3863.

Neufeldt, C.J., Cortese, M., Acosta, E.G., and Bartenschlager, R. (2018). Rewiring cellular networks by members of the Flaviviridae family. Nat. Rev. Microbiol. *16*, 125–142.

Ornitz, D.M., and Itoh, N. (2015). The Fibroblast Growth Factor signaling pathway. Wiley Interdiscip. Rev. Dev. Biol. *4*, 215–266.

Pear, W.S., Nolan, G.P., Scott, M.L., and Baltimore, D. (1993). Production of high-titer helper-free retroviruses by transient transfection. Proc. Natl. Acad. Sci. USA *90*, 8392–8396.

Perera, R., Riley, C., Isaac, G., Hopf-Jannasch, A.S., Moore, R.J., Weitz, K.W., Pasa-Tolic, L., Metz, T.O., Adamec, J., and Kuhn, R.J. (2012). Dengue virus infection perturbs lipid homeostasis in infected mosquito cells. PLoS Pathog. *8*, e1002584.

Reiss, S., Rebhan, I., Backes, P., Romero-Brey, I., Erfle, H., Matula, P., Kaderali, L., Poenisch, M., Blankenburg, H., Hiet, M.S., et al. (2011). Recruitment and activation of a lipid kinase by hepatitis C virus NS5A is essential for integrity of the membranous replication compartment. Cell Host Microbe *9*, 32–45.

Rieber, N., Knapp, B., Eils, R., and Kaderali, L. (2009). RNAither, an automated pipeline for the statistical analysis of high-throughput RNAi screens. Bioinformatics *25*, 678–679.

Ruhe, J.E., Streit, S., Hart, S., Wong, C.H., Specht, K., Knyazev, P., Knyazeva, T., Tay, L.S., Loo, H.L., Foo, P., et al. (2007). Genetic alterations in the tyrosine

kinase transcriptome of human cancer cell lines. Cancer Res. *67*, 11368–11376.

Sanjana, N.E., Shalem, O., and Zhang, F. (2014). Improved vectors and genome-wide libraries for CRISPR screening. Nat. Methods *11*, 783–784.

Savidis, G., McDougall, W.M., Meraner, P., Perreira, J.M., Portmann, J.M., Trincucci, G., John, S.P., Aker, A.M., Renzette, N., Robbins, D.R., et al. (2016). Identification of Zika Virus and Dengue Virus Dependency Factors using Functional Genomics. Cell Rep. *16*, 232–246.

Scaturro, P., Trist, I.M., Paul, D., Kumar, A., Acosta, E.G., Byrd, C.M., Jordan, R., Brancale, A., and Bartenschlager, R. (2014). Characterization of the mode of action of a potent dengue virus capsid inhibitor. J. Virol. *88*, 11540–11555.

Scaturro, P., Stukalov, A., Haas, D.A., Cortese, M., Draganova, K., Płaszczyca, A., Bartenschlager, R., Götz, M., and Pichlmair, A. (2018). An orthogonal proteomic survey uncovers novel Zika virus host factors. Nature *561*, 253–257.

Tang, S., Hao, Y., Yuan, Y., Liu, R., and Chen, Q. (2018). Role of fibroblast growth factor receptor 4 in cancer. Cancer Sci. *109*, 3024–3031.

Urbanowski, M.D., and Hobman, T.C. (2013). The West Nile virus capsid protein blocks apoptosis through a phosphatidylinositol 3-kinase-dependent mechanism. J. Virol. *87*, 872–881.

van Asten, S.D., Raaben, M., Nota, B., and Spaapen, R.M. (2018). Secretome Screening Reveals Fibroblast Growth Factors as Novel Inhibitors of Viral Replication. J. Virol. *92*, e00260-18.

Wang, L., Yang, L., Fikrig, E., and Wang, P. (2017). An essential role of PI3K in the control of West Nile virus infection. Sci. Rep. *7*, 3724.

Webster, M.K., and Donoghue, D.J. (1996). Constitutive activation of fibroblast growth factor receptor 3 by the transmembrane domain point mutation found in achondroplasia. EMBO J. *15*, 520–527.

Welsch, S., Miller, S., Romero-Brey, I., Merz, A., Bleck, C.K., Walther, P., Fuller, S.D., Antony, C., Krijnse-Locker, J., and Bartenschlager, R. (2009). Composition and three-dimensional architecture of the dengue virus replication and assembly sites. Cell Host Microbe *5*, 365–375.

Willemsen, J., Wicht, O., Wolanski, J.C., Baur, N., Bastian, S., Haas, D.A., Matula, P., Knapp, B., Meyniel-Schicklin, L., Wang, C., et al. (2017). Phosphorylation-Dependent Feedback Inhibition of RIG-I by DAPK1 Identified by Kinome-wide siRNA Screening. Mol. Cell *65*, 403–415.e8.

Yu, I.M., Holdaway, H.A., Chipman, P.R., Kuhn, R.J., Rossmann, M.G., and Chen, J. (2009). Association of the pr peptides with dengue virus at acidic pH blocks membrane fusion. J. Virol. *83*, 12101–12107.

Zhang, R., Miner, J.J., Gorman, M.J., Rausch, K., Ramage, H., White, J.P., Zuiani, A., Zhang, P., Fernandez, E., Zhang, Q., et al. (2016). A CRISPR screen defines a signal peptide processing pathway required by flaviviruses. Nature *535*, 164–168.

Zhao, L.J., Wang, W., Wang, W.B., Ren, H., and Qi, Z.T. (2015). Involvement of ERK pathway in interferon alpha-mediated antiviral activity against hepatitis C virus. Cytokine *72*, 17–24.

STAR★METHODS

KEY RESOURCES TABLE

REAGENT or RESOURCE	SOURCE	IDENTIFIER
Antibodies		
rabbit Phospho-FGFR Pan (Tyr653, Tyr654) rabbit Polyclonal Antibody	Thermo fisher	Cat.#PA5-64626; RRID:AB_2662537
Phospho-FGF Receptor (Tyr653/654) (55H2) Mouse mAb	Cell Signaling	Cat.#3476; RRID:AB_331369
FGF Receptor 4 (D3B12) XP® Rabbit mAb	Cell Signaling	Cat.#8562; RRID:AB_10891199
Rabbit anti–phospho-FRS2-α (Tyr196),	Cell Signaling	Cat.#3864; RRID:AB_2106222
Rabbit anti-FRS2 Antibody (H-91)	Santacruz	Cat.#sc-8318; RRID:AB_2106228
Rabbit anti-Phospho-p44/42 MAPK (Erk1/2) (Thr202/Tyr204)	Cell Signaling	Cat.#9101; RRID:AB_331646
Rabbit anti-p44/42 MAPK (ERK1/2)	Cell Signaling	Cat.#9102; RRID:AB_330744
Rabbit anti-Phospho-Akt (Ser473)	Cell Signaling	Cat.#9271; RRID:AB_329825
Akt (pan) (40D4) Mouse mAb	Cell Signaling	Cat.#2920; RRID:AB_1147620
Mouse anti-GAPDH	Santacruz	Cat.#sc365062; RRID:AB_10847862
Mouse anti-Beta Actin	Sigma	Cat.#A5441; RRID:AB_476744
Sheep anti-TGN46	Biorad	Cat.#AHP500GT; RRID:AB_2203291
Rabbit anti-Furin	Thermo Fisher Scientific	Cat.#PA1-062; RRID:AB_2105077
Rabbit anti-Calnexin	Enzo life sciences	Cat.#ADI-SPA-860-F; RRID:AB_11178981
mouse anti-prM	Abcam	Cat.#ab41473; RRID:AB_873758
mouse monoclonal anti-ENV 3H51	ATCC	Cat.#HB46; RRID:CVCL_D292
mouse anti-HA	Sigma Aldrich	Cat.#H3663; RRID:AB_262051
Mouse anti-DENV NS3	Genetex	Cat.#GTX629477; RRID:AB_2801283
DENV Envelope	Genetex	Cat.#GTX127277; RRID:AB_11163414
DENV Capsid	Genetex	Cat.#GTX103343; RRID:AB_1240697
DENV NS4B	Genetex	Cat.#GTX133311; RRID:AB_2728825
DENV prM	Abcam	Cat.#AB41473-1; RRID:AB_873758
dsRNA	Scicons	Cat.#10010500; RRID:AB_2651015
Rabbit anti-DENV Capsid	Welsch et al., 2009	N/A
Rabbit anti-DENV Envelope	Miller et al., 2006	N/A
Rabbit anti-DENV prM	Welsch et al., 2009	N/A
Rabbit anti-DENV NS3	Miller et al., 2006	N/A
Goat anti–rabbit IgG-HRP	Sigma	Cat.#A6154; RRID:AB_258284
Goat anti–rabbit IgG-HRP	Sigma	Cat.#A4416; RRID:AB_258167
Rabbit anti–sheep IgG-HRP	Life technologies	Cat.#31480; RRID:AB_228457
Alexa Fluor 488 donkey anti-rabbit IgG	Thermo Fisher Scientific	Cat.#A-21206; RRID:AB_2535792
Alexa Fluor 488 donkey anti-mouse IgG	Thermo Fisher Scientific	Cat.#A-21202; RRID:AB_141607
Alexa Fluor 488 donkey anti-mouse IgG2a	Thermo Fisher Scientific	Cat.#A-21131; RRID:AB_141618
Alexa Fluor 568 donkey anti-rabbit IgG	Thermo Fisher Scientific	Cat.#A-10042; RRID:AB_2534017
Alexa Fluor 568 donkey anti-mouse IgG	Thermo Fisher Scientific	Cat.#A-10037; RRID:AB_2534013
Alexa Fluor 568 donkey anti-mouse IgG1	Thermo Fisher Scientific	Cat.#A-21124; RRID:AB_141611
Alexa Fluor 647 donkey anti-rabbit IgG	Thermo Fisher Scientific	Cat.#A−31573; RRID:AB_2536183
Alexa Fluor 647 donkey anti-mouse IgG	Thermo Fisher Scientific	Cat.#A-31571; RRID:AB_162542
Alexa Fluor 647 donkey anti-mouse IgG2b	Thermo Fisher Scientific	Cat.#A-21242; RRID:AB_2535811
Donkey anti-Sheep IgG (H+L) Cross-Adsorbed Secondary Antibody, Alexa Fluor 488	Thermo Fisher Scientific	Cat.#A-11015; RRID:AB_141362

(*Continued on next page*)

Continued

REAGENT or RESOURCE	SOURCE	IDENTIFIER
Bacterial and Virus Strains		
DENV isolate 16681, synthetic genome	Fischl and Bartenschlager, 2013	N/A
DENV isolate New Guinea C (NGC)	gift from Dr. Andrew Davidson	N/A
DVs-R2A	Fischl and Bartenschlager, 2013	N/A
DENV serotypes 1, 3, and 4;	Progen Biotechnik GmbH	N/A
Zika virus strains MR766	European Virus Archive (EVAg, France)	Cat.#001v-EVA143
Zika virus strains H/PF/2013	European Virus Archive (EVAg, France)	Cat.#001v-EVA1545
West Nile Virus (NY99)	gift from Jonas Schmidt-Chanasit	N/A
Rift Valley Fever virus (RVFV) encoding a Renilla Luciferase gene	gift from Friedemann Weber	N/A
Chemicals, Peptides, and Recombinant Proteins		
Lipofectamine 2000	ThermoFischer	Cat.#11668019
DAPI-Fluoromount-G	Southern BioTech	Cat.#0100-20
Takyon SYBR green master mix	Eurogentec	Cat.#UF-NSMT-B0710
Transit LT-1 transfection reagent	Mirus	Cat.#MIR2304
Furin	New England Biolabs	Cat.#P8077S
Gelatine	Sigma-Aldrich	Cat.#G-9391
DAPI	Thermo Fisher Scientific	Cat.#D1306; RRID:AB_2629482
Boc-Arg-Val-Arg-Arg-AMC acetate salt	Bachem	Cat.#I-1645.0025
PD173074	Sigma Aldrich	Cat.#P2499
LY294002	Sigma Aldrich	Cat.#L9908
U0126	Sigma Aldrich	Cat.#19-147
Cycloheximide	Sigma Aldrich	Cat.#C7698
Critical Commercial Assays		
Silencer® Human Kinase siRNA Library V3	Ambion, ThermoFischer	Cat.#AM80010V3
High-Capacity cDNA Reverse Transcription Kit	ThermoFischer	Cat.#4368814
CellTiter-Glow	Promega	Cat.#G9241
Experimental Models: Cell Lines		
Huh7 (male)	Nakabayashi et al., 1982	N/A
Huh7-FurinKO (male)	This paper	N/A
HEK293T (female)	ATCC	Cat.#CRL-3216; RRID:CVCL_0063
HeLa (female)	ATCC	Cat.#ATCC CCL-2; RRID:CVCL_0030
C6/36 (sex not defined)	ATCC	Cat.#CRL1660; RRID:CVCL_Z230
Vero clone E6 (female)	ATCC	Cat.#CRL1586; RRID:CVCL_0574
Oligonucleotides		
Primers for FGFR4_K645E_HA Fw:CATTGACTACTATAAGgagACCAGCAACGGCCGCC Rv:GGCGGCCGTTGCTGGTctcCTTATAGTAGTCAATG	This study	N/A
Primers for FGFR4_Y367C_HA Fw:CGCCCGAGGCCAGGtgcACGGACATCATCCT Rv:AGGATGATGTCCGTgcaCCTGGCCTCGGGCG	This study	N/A
Oligo sequence for furin KO cells generation: CGTACCAGGTACCACTGCTG	This study	N/A
Recombinant DNA		
pCMV-Gag-Pol	Gift from Didier Trono	N/A
pMD2-VSV-G	Gift from Didier Trono	N/A

(*Continued on next page*)

Continued

REAGENT or RESOURCE	SOURCE	IDENTIFIER
pWPI_FGFR4_ K645E _HA	This paper	N/A
pWPI_FGFR4_ Y367C_HA	This paper	N/A
pWPI_prM-E	Scaturro et al., 2014	N/A
pWPI_Capsid	Scaturro et al., 2014	N/A
pFurinKO-4	This paper	N/A
pVSV-G_ts045_GFP	Gift from Megan Stanifer.	N/A
Software and Algorithms		
ImageJ		https://imagej.nih.gov/ij/
Adobe Photoshop 5.5	San Jose, CA, USA	N/A
GraphPad Prism 5.0	LaJolla, CA, USA	N/A
RNAither	Rieber et al., 2009	https://bioconductor.org/packages/release/bioc/html/RNAither.html

CONTACT FOR REAGENT AND RESOURCE SHARING

Further information and requests for resources and reagents should be directed to and will be fulfilled by the Lead Contact, Ralf Bartenschlager (ralf.bartenschlager@med.uni-heidelberg.de).

Plasmids and/or cell lines will be distributed under the terms of a material transfer agreement.

EXPERIMENTAL MODEL AND SUBJECT DETAILS

Cell lines and culture conditions

The mammalian cell lines Huh7 (Nakabayashi et al., 1982), HEK293T (Pear et al., 1993; DuBridge et al., 1987) and Vero clone E6 (ATCC® CRL1586) were grown in Dulbecco's modified minimal essential medium (DMEM; Invitrogen, Karlsruhe, Germany) supplemented with 2 mM L-glutamine, nonessential amino acids, 100 U/ml penicillin, 100 μg/ml streptomycin, and 10% fetal calf serum in a 37°C incubator with 5% CO_2. The *Aedes albopictus* clone C6/36 (ATCC® CRL1660) was maintained in minimal essential medium (MEM; Invitrogen) supplemented with 10 mM HEPES [pH 7.4], 2 mM L-glutamine, nonessential amino acids, 100 U/ml penicillin, 100 μg/ml streptomycin, and 10% fetal calf serum at 28°C. Origin and sex of all cell lines are stated in the Key Resources Table.

Viruses

The molecular clone of the DENV isolate 16681 has been reported previously (Fischl and Bartenschlager, 2013). The cloned genome of the DENV isolate New Guinea C (NGC) was a kind gift from Dr. Andrew Davidson, University of Bristol, UK (Gualano et al., 1998). The Zika virus strains MR766 and H/PF/2013 were obtained from the European Virus Archive (EVAg, France). All virus stocks were prepared by amplification in C6/36 insect cells and virus titers were determined by plaque assay using Vero cells.

METHOD DETAILS

Plasmid constructions

Plasmids containing the full length DENV2 16681 sequence as well as the Renilla luciferase reporter virus and the sub-genomic reporter replicon, both derived from the 16681 isolate, have been described elsewhere (Fischl and Bartenschlager, 2013). The human FGFR4 gene was amplified from the human ORFeome collection and inserted into the lentiviral plasmid vector pWPI using the Gateway recombination system (Invitrogen). To generate the constitutive active mutants, site directed mutagenesis was performed using the Quickchange II system (Agilent, Santa Clara, CA) with the FGFR4 wild-type sequence as template and the following primers: 5′CGCCCGAGGCCAGGtgcACGGACATCATCCT3′ and 5′AGGATGATGTCCGTgcaCCTGGCCTCGGGCG3′ for the Y367C mutant and 5′CATTGACTACTATAAGgagACCAGCAACGGCCGCC3′ and 5′GGCGGCCGTTGCTGGTctcCTTATAGTAGT CAATG3′ for the K645E mutant. In all constructs a hemagglutinin (HA) tag was added in-frame to the 5′ end of the FGFR4 coding sequence.

Primary siRNA Screening

The primary screening was performed by reverse transfection cell arrays with a human siRNA kinome library as described elsewhere (Erfle et al., 2007; Willemsen et al., 2017; Reiss et al., 2011). This library targets all known and predicted 719 human kinases with three individual siRNAs per gene (Silencer® Human Kinase siRNA Library V3, AM80010V3; Ambion, ThermoFischer Scientific). Briefly, the

siRNA-gelatin transfection solution was prepared in 384-well plates (Nalgene-Nunc) by mixing 5 μL of a 30 μM siRNA stock solution with 3.5 μL of Lipofectamine 2000 (Invitrogen) and 3 μL Opti-MEM (Invitrogen) containing 0.4 M sucrose using an automated liquid handler (MICROLAB STAR, Hamilton). After 20 min incubation at room temperature, 7.25 μL of 0.2% gelatine (G-9391, Sigma-Aldrich) and 0.01% (v/v) fibronectin (Sigma-Aldrich) was added to the mixture. This solution was arrayed onto single-well-chambered Lab-Tek cover glass tissue culture dishes (Nalgene-Nunc) using a contact printer (Chip Writer 'Compact' and 'Pro', Bio-Rad laboratories) with PTS600 solid pins (Point Technologies, Boulder, CO) resulting in a spot diameter of approximately 400 μm and a center-to-center spot distance of 1.125 μm. The spot volume was approximately 4 nl. Lab-Tek chamber glasses were dried in plastic boxes containing silica gel (Merck) at least overnight prior to use. After spotting, the first and last spot on the grid were marked with visual ink on the outside of the glass to allow precise positioning of the microscope for image analysis of the exact spot area.

Huh7 cells were seeded onto the arrayed chamber slides at a density of $1.5x10^5$ cells per chamber. After 48 h incubation, cells were infected with the DENV2 NGC strain using a MOI of 5. The slides were harvested 24 h post-infection and processed for immunostaining. After several times washing with PBS, cells were fixed with 2% paraformaldehyde (Sigma Aldrich) and permeabilized with 0.5% Triton X-100 (Merk). Primary antibody (anti-E, diluted 1:100) and secondary antibody (anti-mouse Alexa Fluor 546, diluted 1:500) (Invitrogen, A11030) were prepared in PBS, supplemented with 3% normal goat serum. Both antibodies were incubated for 45 min each and the staining procedure was repeated twice to improve the signal intensity. Nuclei were visualized by staining the DNA with DAPI (4',6'-diamidino-2-phenylindole dihydrochloride) (Molecular Probes, Karlsruhe, Germany). Slides were stored in PBS containing 0.05% sodium azide until use. The images of individual siRNA spots were captured using an Olympus scanning microscope (scan˙R, Olympus Biosystems) with a 10X objective. Acquired images were analyzed as described elsewhere (Matula et al., 2009). For each experiment technical duplicates were performed and a total of six independent experiments were carried out. Only siRNA spots containing more than 125 cells and less than 500 cells were included in the analysis. As additional quality control for staining artifacts, all images were analyzed by eye and an additional 15% of the images and three experimental sets were excluded from the final analysis. Statistical analysis of processed imaging data was carried out in R Version 2.8.0 (R Development Core Team, http://www.R-project.org), using the Bioconductor packages RNAither (Rieber et al., 2009) and cellHTS (Livak and Schmittgen, 2001). In brief, locally weighted scatterplot smoothing (LOWESS) was used to normalize the signal intensities for effects of differing cell counts (Matula et al., 2009). Spatial effects within individual LabTeks were removed by B-score normalization (Rieber et al., 2009) and the variability between plates was normalized by subtracting the plate median from each measurement and dividing by the plate median absolute deviation. For statistical analysis, Z-scores were calculated from the mean signals over replicates and the *p-value*s were calculated for each siRNA using Student's t test. Replicates were summarized using the mean; furthermore, a t test was carried out to determine whether siRNA effects differed significantly from zero. The mean score indicates the magnitude of an effect, whereas the p value is a measure of the reproducibility. A knock-down was scored positive when its p value was < 0.05 and its Z-score lower than -1 in case of dependency factors or higher than +1 in case of restriction factors. This combination of *p-value* and score allows the identification of genes with a relatively small, but consistent effect.

Validation siRNA screening

For validation of primary hits, reverse transfection of siRNAs in a 96-well plate format was used as described elsewhere (8). For each of the 110 kinases three new siRNAs were purchased from Dharmacon (Horizon, UK). In brief, the transfection mix was prepared by mixing 3 μl OptiMEM (containing 0.4 M sucrose) with 3.5 μl Lipofectamine 2000 (Invitrogen) and 5 μl of the respective siRNA (30μM stock) in a 384-well plate using an automated liquid handler. After incubation for 20 min at room temperature, 7.25 μl of a 0.08% (w/v) gelatin solution containing 0.01% (v/v) fibronectin were added to the mixture and 17 μl of the source siRNA transfection solution were transferred into a 96-well plate and combined with 850 μl of MilliQ water. Fifty-one μl of the transfection mixture were transferred into each well of a 96-well plate (Greiner, cat. no. 655098) and plates were dried for 2.5 h at medium drying force in a multiwell Speed Vac. Huh7 cells (5,000 cells per well) were seeded into siRNA-coated 96-well plates in a volume of 100 μl per well. Twenty four hours later cells were inoculated with the DV-R2A Renilla luciferase reporter virus at an MOI of 0.5 and medium was exchanged 4 h later. Fourty eight hours post infection, cells were harvested in 50 μl luciferase lysis buffer (1% (w/v) Triton X-100, 25 mM glycylglycine [pH 7.8], 15 mM $MgSO_4$, 4 mM EGTA and 1 mM DTT). Plates were measured using home-made substrates for Renilla luciferases as described elsewhere (Fischl and Bartenschlager, 2013). The validation screening was performed twice in duplicates and statistically analyzed as follows. Signal intensities normalized for cell count effects using locally weighted scatterplot smoothing, were normalized to the negative controls by subtracting the median signal of the negative controls from each measurement and dividing by the median absolute deviation of the negative controls. Replicates were summarized using the mean and hits were defined based on a score threshold of ± 2.0 for at least one siRNA per gene.

Electroporation of DENV RNA

In vitro transcripts were generated as previously described (Chatel-Chaix et al., 2015) and used for electroporation of single cell suspensions of either BHK21 or Huh7 cells that were generated by trypsinization. Cells were washed once with PBS and suspended in cytomix containing 2 mM ATP and 5 mM glutathione at a density of 1.5×10^7 or 1.0×10^7 cells per ml, respectively. Ten μg of *in vitro*-transcribed RNA was mixed with 400 μl of cell suspension and cells were electroporated using a Gene Pulser system (Bio-Rad) in a cuvette with a gap width of 0.4 cm (Bio-Rad) at 960 μF and 270 V. Cells were immediately transferred into complete DMEM and seeded into appropriate formats.

Virus replication assays

For inhibition experiments, cells were pre-treated for 16 h with given compounds prior to infection. Inhibitors were present during infection and all time thereafter. Cells plated in duplicate wells of 6-well plates were lysed at given time points in 350 μl lysis buffer (1% Triton X-100, 25 mM glycylglycine, 15 mM $MgSO_4$, 4 mM EGTA and 1 mM DTT [pH 7.8]) using repetitive freeze-thaw cycles. For each well, two times 100 μl lysate was mixed with 360 μl assay buffer (25 mM glycylglycine, 15 mM $MgSO_4$, 4 mM EGTA, 1 mM DTT, 2 mM ATP and 15 mM K_2PO_4, [pH 7.8]) and, after addition of 200 μl of a luciferin solution (200 μM luciferin, 25 mM glycylglycine [pH 8.0]), measured for 20 s in a luminometer (Lumat LB9507; Berthold, Freiburg, Germany). Replication kinetics were determined by normalizing the relative light units (RLU) measured at different time points after transfection to the 4 h value that reflects translation from the input RNA and thus transfection efficiency.

RNA quantification by RT-qPCR

Total cellular RNA from around 5 × 10^5 virus-infected cells was isolated using the Nucleo Spin RNAII kit (Macherey-Nagel, Düren, Germany) as recommended by the manufacturer. cDNA was generated using the High Capacity cDNA RT kit (4368814, Applied Biosystems, ThermoFisher scientific). Quantitative PCR was done using an ABI PRISM 7000 sequence detector system (Applied Biosystems, Foster City, CA). For each primer set, reactions were conducted in triplicate using the Green Dye RT-PCR master mix (PJK GmbH, Hilden, Germany) according to the instructions of the manufacturer and the following primers: forward - 5′TTG AGTAAACTGTGCAGCCTGTAGCTC3′ and reverse - 5′GGGTCTCCTCTAACCTCTAGTCCT3′ (DENV); forward - 5′GAAGGTGAAG GTCGGAGT3′ and reverse - 5′GGGTCTCCTCTAACCTCTAGTCCT3′ (GAPDH). The total volume of the reaction mix was 15 μl and reactions were performed in three stages: stage 1, 15 min at 95°C; stage 2, 40 cycles with each 15 s at 95°C and 60 s at 60°C. Quantities of DENV RNA were calculated by using serial dilutions of known amounts of DENV *in vitro* transcripts that were processed in parallel. For cellular genes, the ΔΔCT method (5) was used to calculate the relative expression levels.

Indirect immunofluorescence

Huh7 cells were seeded onto glass coverslips in 24-well plates (6x10^4 cells/well). After 16 h, cells were treated with different chemical inhibitors as specified in the results section, and 8 h later infected with DENV2 for one hour in the presence of the inhibitors. At different time points post-infection, cells were fixed with 4% paraformaldehyde (Applichem GmbH, Darmstadt, Germany) and permeabilized with 0.5% (v/v) Triton X-100 in PBS. Primary staining was done by 45 min incubation with primary antibodies diluted in PBS containing 10% normal goat serum. After several washes with PBS, secondary staining was done by 45 min incubation with an Alexa-conjugated secondary antibody, diluted 1:1,000 in PBS containing 10% goat serum. Nuclear DNA was stained with DAPI (Molecular Probes). Samples were mounted onto glass slides with Fluoromount G (Southern Biotechnology Associates, Birmingham, USA) and images were acquired using a Nikon Eclipse Ti spinning disc confocal laser microscope or a Leica confocal SP8. Images were processed and quantified using the ImageJ software package (National Institute of Health, Bethesda, MD, USA).

Lentivirus production and FGFR4 overexpression

For lentivirus production, 293T cells were transfected with the packaging plasmids pCMV-Gag-Pol and pMD2-VSV-G (kind gifts from Didier Trono, EPFL, Lausanne, Switzerland) together with the pWPI vector coding for the different FGFR4 proteins by using polyethylenimine (Polysciences Inc.). Two days post-transfection, lentivirus-containing supernatant was harvested and filtered through a 0.45 μm pore-size filter. Virus titers were determined by transduction of HeLa cells using serial dilutions of the lentivirus preparation and selection with 1 μg/ml puromycin. Cells were fixed five days later and stained with 1% crystal violet/10% ethanol for 30 min. After extensive rinsing with water, cell colonies were counted and titers were calculated. For FGFR4 mutants overexpression, Huh7 cells were transduced using an MOI of 5 for three days prior to infection with wild-type DENV (MOI = 0.1) or DV-R2A (MOI = 1).

Generation of trans-complemented DENV particles

Production of trans-complemented DENV particles ($DENV_{TCP}$) was performed as previously described (Scaturro et al., 2014). Briefly, 10 μg of *in-vitro* transcribed DV-R2A subgenomic RNA were electroporated into 293T cells. After 24 h, cells were transduced with lentiviruses encoding for prM-E and capsid. Temperature was shifted to 33°C, supernatants were collected at day 4 and day 6 post-transduction, pooled and filtered through a 0.44 μm pore-size filter.

Generation of furin KO cells

To have a cell line that could be used as negative control in our furin assays, we generated furin knock-out Huh7 cells. The guide RNA sequence for furin was taken from a public database (GeCKO library, (Sanjana et al., 2014)). Complementary synthetic oligonucleotides of the desired sequence (5′CGTACCAGGTACCACTGCTG′3) were annealed and inserted into the lentiCRISPRv2 plasmid containing a puromycin resistance gene. Lentiviruses were generated as described above and Huh7 cells were transduced using an MOI of 5. Selection was started 24 h after transduction with 3 μg/ml puromycin. Drug resistant cell pools were expanded and furin knock-out was validated by western blot.

Electron microscopy

Huh7 cells were treated for 16 h with FGFR and PI3K inhibitors (PD173074 and Ly294002, respectively) or DMSO, and mock-infected or infected with DENV in the presence of the inhibitors. Cells were fixed 72 h later with EM fixative (2.5% glutaraldehyde in 50 mM cacodylate, 50 mM KCl, 2.6 mM $CaCl_2$, 2.6 mM $MgCl_2$, 2% sucrose) for at least one hour at room temperature and embedded in epoxy resin as previously described (Cortese et al., 2017). Samples were examined with a TEM Zeiss 10C electron microscope (Carl Zeiss, Oberkochen) at 80 kV and images analyzed using the ImageJ software package.

Cell fractionation

All steps of the fractionation procedure were carried at 4°C. Huh7 cells seeded into 15 cm-diameter dishes (1.5x 10^7 cells/dish) were left untreated or treated with the FGFR4 inhibitor PD173074 (0.6 μM) or the PI3K inhibitor LY294002 (10 μM), and infected with DENV. Forty-eight hours later, cells were scraped into ice-cold PBS, and centrifuged for 10 min at 700xg. Cell pellets were gently resuspended in 1 mL HOP buffer (50 mM Tris-HCl [pH 7.5], 120 mM NaCl, 30 mM KCl, 3 mM EDTA) and dissociated as previously described (Bär et al., 2013). Nuclei were separated by centrifugation at 1000xg for 5 min, clarified supernatants were adjusted to 2 mL and centrifuged through a Nycodenz step-gradient (2 mL 30%, 1.33 mL 20%, 1.33 mL 15%, 1.33 mL 10%, 1.33 mL 7.5%, 1.33 mL 5%, 1.33 mL 2.5% (w/v) Nycodenz in HOP) at 33000xg for 15 min in a SW40 rotor (Beckman, Pasadena, CA). Eight fractions of 1.33 mL were collected from the top of the gradient and analyzed by western-blot or plaque assay.

Furin cleavage assay

Purified immature virus particles were treated with furin as described earlier (Yu et al., 2009). Briefly, Huh7 cells grown in 10 cm-diameter dishes were infected with DENV (MOI = 3). After 24 h, medium was replaced by complete DMEM containing 20 mM NH_4Cl. Supernatants were harvested 48 h post-infection and virus particles were concentrated by ultracentrifugation through a 20% sucrose cushion in NTE buffer (100 mM NaCl, 10 mM Tris-HCl [pH 8.0], 1 mM EDTA) for 4 h at 24,000 rpm in a SW32 Ti rotor (Beckman) at 4°C. Virus containing pellets were resuspended in NTE buffer. Samples were mixed with an equal volume of 50 mM 2-(N-morpholino)ethanesulfonic acid (MES) to adjust the pH to 6.0 and 4 units of purified Furin (New England Biolabs, P8077) in a final concentration of 3 mM $CaCl_2$. After 16 h incubation at 30°C, the reaction was terminated by neutralization of the pH using one volume of 100 mM Tris [pH 8.0] and 120 mM NaCl.

Furin enzyme activity assay

Huh7 cells seeded in 96 well black plate, were pre-treated for 16 h with compounds and infected with DENV2 (MOI = 0.1) or mock infected. After 72 h, cells were washed in PBS three times and incubated for 4 h in assay buffer (DMEM without phenol-red, 100 μM furin fluorogenic substrate BOC-RVRR-AMC, 0.25% Triton X-100). After cell lysis, samples were diluted 1:4 in PBS and incubated for additional 24 h at room temperature. Fluorescence was measured using 380 nm for excitation and 460 nm emission recording. Data were normalized to cell density (calculated by measurement of ATP levels on a culture plate treated in parallel) and normalized to values obtained with DMSO treated control cells. Furin knock-out cells were used as positive control to confirm the specificity of the furin assay.

VSV-G trafficking assay

Huh7 cells were transfected with the VSV-G_ts045_GFP construct. After 6 h medium was replaced by imaging medium containing 0.6 μM PD173074 or DMSO and temperature was increased to 40°C. Two hours before imaging, 100 μM cycloheximide was added to the cells. Cells were imaged 24 h post-transfection at 32°C with a confocal spinning disc microscope. For each cell, a single confocal slice was collected every 5 min. For each time point, the fluorescence intensity in a region of interest surrounding the perinuclear area was calculated and normalized to the intensity at time point 0.

QUANTIFICATION AND STATISTICAL ANALYSIS

All statistical analyses were performed with the GraphPad Prism 5.0 software package (LaJolla, CA, USA). To assess statistical significance, both the two-tailed paired Student's t test with Bonferroni correction for multiple samples comparison or one-way ANOVA and Dunnett's post hoc test analysis were used. Datasets were considered significantly different if the P value was less than 0.05. For each experiment, the statistical analysis performed and the sample sizes are listed in figure legends.